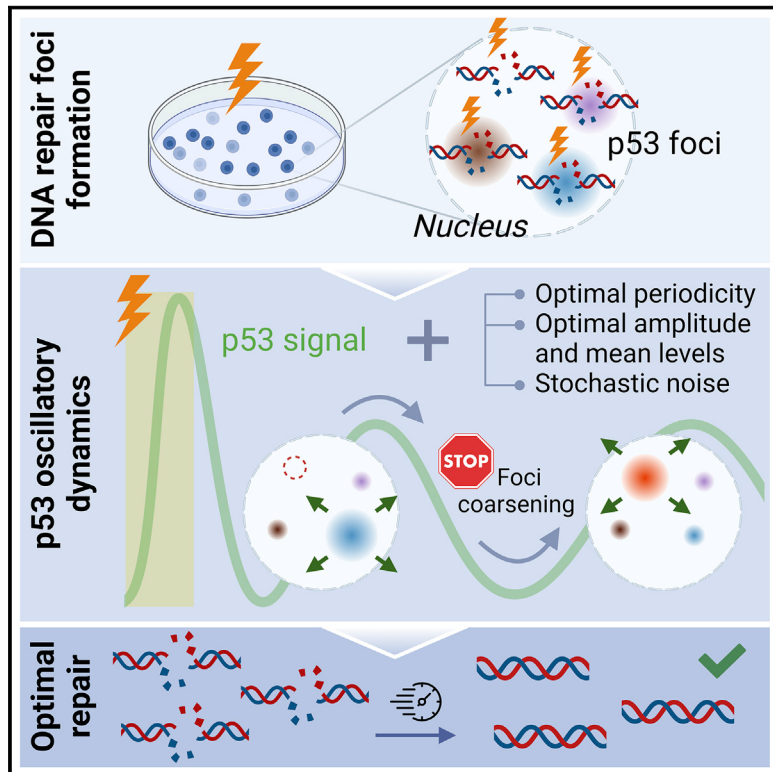


Enhanced DNA repair through droplet formation and p53 oscillations

Graphical abstract



Authors

Mathias S. Heltberg,
Alessandra Lucchetti, Feng-Shu Hsieh,
Duy Pham Minh Nguyen,
Sheng-hong Chen, Mogens H. Jensen

Correspondence

mathias.heltberg@nbi.ku.dk (M.S.H.),
mhjensen@nbi.dk (M.H.J.)

In brief

A theory explains how oscillations in p53 nuclear abundance optimize DNA damage repair.

Highlights

- p53 oscillations optimize DNA repair compared to cells with sustained levels
- Enhanced DNA repair efficiency may be achieved by suppression of Ostwald ripening
- Natural p53 periodicity and amplitude enable optimal distribution of repair material
- Oscillations enhance robustness of DNA damage response in stochastic environments



Theory

Enhanced DNA repair through droplet formation and p53 oscillations

Mathias S. Heltberg,^{1,4,*} Alessandra Lucchetti,^{1,4} Feng-Shu Hsieh,² Duy Pham Minh Nguyen,² Sheng-hong Chen,^{2,3} and Mogens H. Jensen^{1,5,*}

¹Niels Bohr Institute, University of Copenhagen, Copenhagen, 2100, Denmark

²Lab for Cell Dynamics, Institute of Molecular Biology, Academia Sinica, Taipei, 115, Taiwan

³National Center for Theoretical Sciences, Physics Division, Complex Systems, Taipei, 10617, Taiwan

⁴These authors contributed equally

⁵Lead contact

*Correspondence: mathias.heltberg@nbi.ku.dk (M.S.H.), mhjensen@nbi.dk (M.H.J.)

<https://doi.org/10.1016/j.cell.2022.10.004>

SUMMARY

Living organisms are constantly exposed to DNA damage, and optimal repair is therefore crucial. A characteristic hallmark of the response is the formation of sub-compartments around the site of damage, known as foci. Following multiple DNA breaks, the transcription factor p53 exhibits oscillations in its nuclear concentration, but how this dynamics can affect the repair remains unknown. Here, we formulate a theory for foci formation through droplet condensation and discover how oscillations in p53, with its specific periodicity and amplitude, optimize the repair process by preventing Ostwald ripening and distributing protein material in space and time. Based on the theory predictions, we reveal experimentally that the oscillatory dynamics of p53 does enhance the repair efficiency. These results connect the dynamical signaling of p53 with the microscopic repair process and create a new paradigm for the interplay of complex dynamics and phase transitions in biology.

INTRODUCTION

Living organisms need to have highly specialized and optimized responses to external stresses, as a result of which many transcription factors (TFs) portray a complex dynamics. Indeed, decades of research in the field have shown how proteins such as nuclear factor κ B (NF- κ B) (Hoffmann et al., 2002; Nelson et al., 2004), Hes1 (Kobayashi et al., 2009), and p53 (Lahav et al., 2004) show oscillations in their nuclear concentration with periods on the timescale of hours. A typical quantitative approach consists of studying the underlying biochemical network structure and formulating coupled differential equations in order to understand the occurrence of these oscillations (Tiana et al., 2002; Jensen et al., 2003; Geva-Zatorsky et al., 2006). However, as of today surprisingly little effort has been made to investigate what advantages the cell may gain by exhibiting this dynamics, and this fundamental question has been too often left for qualitative discussions (Heltberg et al., 2021a). It has previously been revealed how large amplitudes can stimulate groups of downstream genes (Heltberg et al., 2016, 2019b), but how the most fundamental trace of oscillations—the periodicity—may be beneficial has been largely overlooked. It would be evolutionary surprising if these oscillations, occurring in some of the most vital TFs, did not serve a distinct role, and it is therefore crucial that biological research applies the biophysical foundations to investigate why the cell has included such dynamical response in specific situations.

In this context, the tumor suppressor protein, p53, is a master regulator of DNA damage response, stimulating numerous genes related to DNA repair. When the cell is exposed to DNA damage, through for instance chemical components or radiation, p53 nuclear concentration is typically elevated. However, following multiple DNA double-strand breaks (DSBs), it exhibits sustained oscillations with a well-defined period of approximately 5.5 h (Lahav et al., 2004; Chen et al., 2016). These oscillations mainly originate as a result of the negative feedback loop with the downstream target Mdm2, even though several other proteins play a role in this loop (Batchelor et al., 2008; Heltberg et al., 2019a).

While the process of DNA repair is complicated, involving a large number of steps, one characteristic hallmark of the response to DSBs is the formation of small sub-compartments rich of repair proteins around the site of damage (Lisby et al., 2004). These have been named ionizing radiation-induced foci (IRIF) and will be referred to simply as foci in this paper. Recently it has been shown that repair foci have properties similar to liquid droplets, and their formation can therefore be described as a second-order phase transition (Oshidari et al., 2020; Miné-Hatab et al., 2021; Pessina et al., 2019; Kilic et al., 2019).

The main focus of this paper is to investigate how the features of liquid droplets can affect the reaction rates of repair proteins in the diffusion-limited regime, and consequently, how the formation of foci can enhance the DNA repair process. In the presence of



multiple liquid droplets, only the largest can grow due to the process of Ostwald ripening. Therefore, serious problems arise when the cell needs to repair multiple damaged sites. What we discovered is that this issue is resolved directly by the presence of oscillations in the TF p53. First, we investigated the case of fast droplet formation, in which case we revealed an optimal period similar to the one found in p53. Secondly, we investigated the regime of slowly forming droplets, where oscillations lead to stabilization of droplet sizes depending on the concentration of proteins to form liquid droplets. Then, we used these results in combination with the mathematical modeling of p53, outlining how single parameters perturbations might alter the underlying repair process. Finally, we tested experimentally the very fundamental hypothesis of the theory—i.e., that p53 oscillations enhance the efficiency of DNA repair—and discovered a significantly reduced level of DNA damage in cells with p53 oscillations. Hence, this work introduces a new role for p53 oscillations and establishes a bridge between the dynamical properties of a TF and the microscopic processes of droplet formation and DNA repair.

RESULTS

Repair of DNA damage through droplet formation

Following multiple DSBs, the cell needs to respond as quickly and efficiently as possible through the process of repairing the damaged sites, by distributing resources at the right position at the right time (Figure 1A). In this context, the three main players that characterize the building blocks of our model are:

- (1) the p53 oscillatory dynamics,
- (2) the formation of liquid foci, and
- (3) the actual process of damage repair.

The experimental oscillatory trace of p53 (Figure 1B), which arises following multiple DSBs, can be reproduced by modeling the negative feedback loop between p53 and Mdm2, as shown for instance by Mengel et al. (2010). In this model, the period and amplitude can be altered by small changes in the parameters, allowing fine-tuned oscillations (Figure 1C). p53 then stimulates the production of repair proteins, which may segregate into liquid droplets, the repair foci, giving rise to an uneven concentration c in the cell nucleus (of radius r_n and volume V_n). It has recently been observed that p53 rapidly accumulates at DSBs sites and directly recruits repair proteins to the foci, suggesting that p53 itself may have significant transcription-independent functions in the DNA damage response (Wang et al., 2022a). Due to the microscopic interactions, proteins will have energetically favorable states inside the droplet, resulting in a lower free energy in this region and therefore in a much higher concentration inside the droplet than right outside it (Figure 1D). In the presence of multiple foci, a fascinating interplay occurs known as Ostwald ripening (Lifshitz and Slyozov, 1961; Wagner, 1961; Hyman et al., 2014; Nishanov and Sobyanin, 1986), where all droplets larger than a critical radius grow, while all the others shrink. Since the critical radius changes accordingly, only one dominating droplet exists in the end. In the presence of N damaged sites and thereby N droplets—assumed to be spherical and far apart from each other—their surrounding can be considered to

be spherically symmetric with a common concentration $c_\infty(t)$ far away from each droplet, which depends on time and mediates the interactions between them. Therefore, the change of radius of the i -th droplet R_i is given by Lifshitz and Slyozov (1961)

$$\frac{dR_i}{dt} = \frac{Dc_{out}}{c_{in}} \frac{1}{R_i} \left(\frac{c_\infty(t)}{c_{out}} - 1 - \frac{l_\gamma}{R_i} \right), \quad (1)$$

where D is the diffusion coefficient outside the droplet, $c_{in,out}$ are the concentrations inside/outside the droplets in the limit $R \rightarrow \infty$ and l_γ is the capillary length. Material conservation dictates that material is shared between the droplets, of volume V_i and internal concentration c_{in} , and the dilute phase, which occupies the volume $V_n - \sum_i^N V_i$ and has a concentration given by c_∞ . Therefore, the average concentration \bar{c} in the total volume V_n is given by:

$$\bar{c}V_n = c_{in} \sum_i^N V_i + c_\infty(t) \left(V_n - \sum_i^N V_i \right). \quad (2)$$

Recently, it was discovered that the DNA repair foci do follow the predictions of the Lifshitz-Slyozov theory to a surprising level. After initial nucleation and growth of droplets, coarsening eventually took place, where small droplets dissolved while large droplets continued to grow, with a rate of the radius $R \propto t^{1/3}$. Furthermore, it was revealed that coarsening predominantly happened without physical contact among the droplets, thereby due to Ostwald ripening, with a timescale of a few hours (Pessina et al., 2019).

To link the formation of liquid foci to p53, we assumed that the concentration of proteins responsible for droplet formation (\bar{c}) linearly follows the p53 concentration.

Simulating the system (Equation 1 and 2) with constant p53 levels—therefore constant \bar{c} —results in a metastable system with one dominating droplet. This is shown in Figure 1E, where the radius of each droplet is portrayed in a different color, matching the schematic representation of Figure 1D. Here, we used the Gillespie algorithm to simulate the evolution of droplet sizes in a stochastic environment (see STAR Methods).

Lastly, we considered the process of DNA damage repair on a single site as a Markov chain consisting of M steps, which need to be sequentially made in order to retrieve the intact DNA (Hahnfeldt et al., 1992; Mohseni-Salehi et al., 2020). Each step is accomplished at a certain rate $1/\tau$, but it can also be reversed at another constant rate λ , until the site is fully repaired (Figure 1F). To calculate the repair rate $1/\tau$, we assumed that this was diffusion limited, allowing us to use first passage time calculations in the Smoluchowski limit (see STAR Methods). Here, we applied a previously derived theory (Helberg et al., 2021b) of how the presence of a droplet can alter the first passage time of a molecule, leading to an optimal droplet size that reduces the search time maximally (Figure 1G). If the free energy is significantly lowered inside the droplet, this equation takes the form

$$\tau = \frac{R^3}{3D_0 r_0} + \frac{r_n^3}{3DR}. \quad (3)$$

where R is the radius of the droplet, D is the diffusion coefficient in the nucleus, D_0 is the diffusion coefficient inside the droplet,

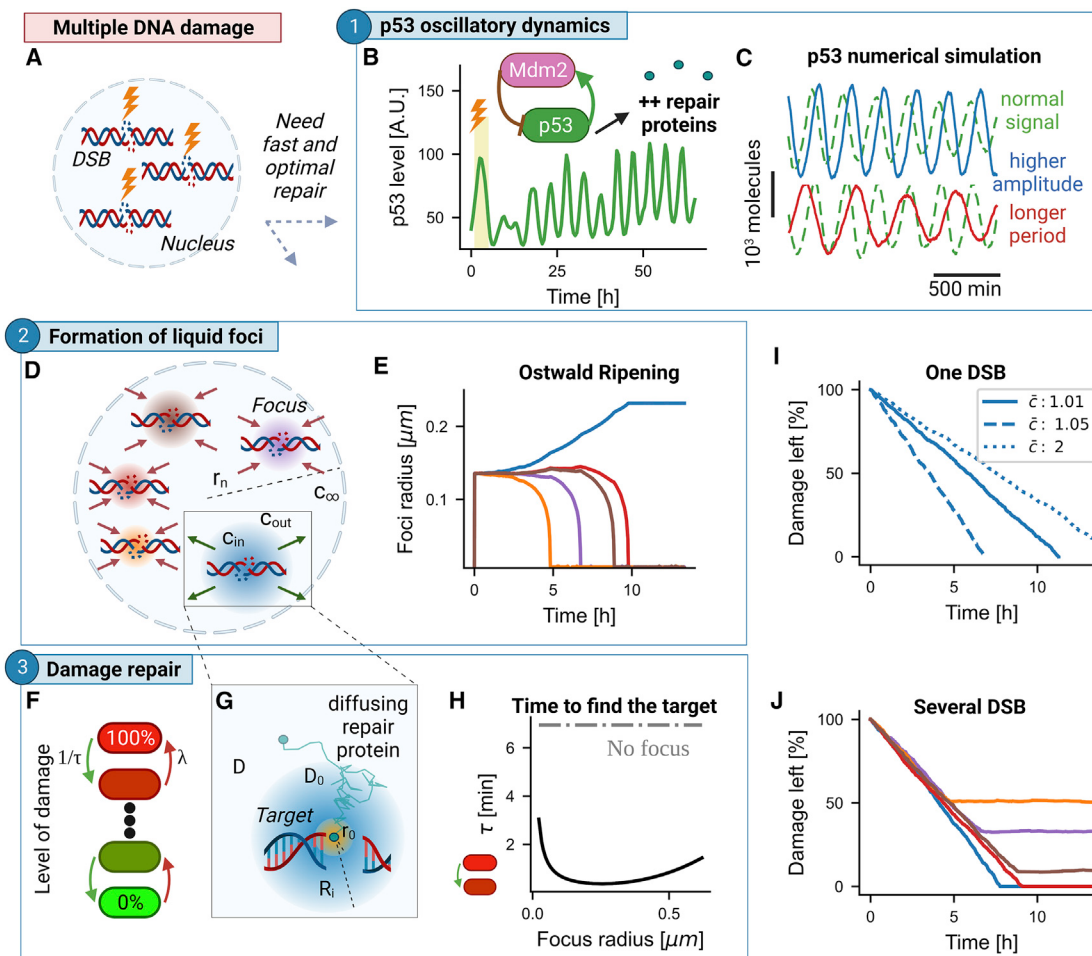


Figure 1. Multiple DNA damage induces p53 oscillatory dynamics and the formation of liquid foci

- (A) Schematic figure showing multiple DNA double-strand breaks (DSBs) in the nucleus of a cell following irradiation.
- (B) Experimental trace of p53 following irradiation. The oscillatory dynamics is believed to stem mainly from the negative feedback loop between p53 and Mdm2. p53 then stimulates the production of repair proteins.
- (C) Simulations of the p53 network, where oscillations occur and periodicity and amplitude may be varied by modifying the parameters of the network.
- (D) Schematic figure showing the formation of foci around the sites of damage and the parameters related in the process. Each droplet is represented by a different color. Arrows indicate whether droplets are shrinking (red) or growing (green).
- (E) The process of Ostwald ripening with one final dominating droplet shown by plotting the individual radii as a function of time. Same color code as in (D).
- (F) Schematic figure showing the DNA repair at a specific site as a discrete Markov chain.
- (G) Schematic figure revealing the droplet around a site of damage and the parameters related in the process.
- (H) First passage time for repair molecules to find a target as a function of the size of the focus (Equation 3). The gray dotted line indicates the time to find a target in the absence of foci (Equation 4).
- (I) The damage as a function of time when only one site is damaged. The three lines indicate different constant average concentrations for the repair proteins. In the legend, \bar{c} is expressed in units of c_{out} .
- (J) The damage as a function of time when five sites are damaged. Same color code as in (D) and (E).
- See Table S1 for the specific parameters used in this figure.

and r_0 is the radius of the site of interest (Figure 1H, black line). In the absence of foci, it reduces to the time it takes to find the target from the edge of the nucleus, which corresponds to the constant value (Figure 1H, gray dashed-dotted line)

$$\tau_{no\ focus} = \frac{r_n^3}{3Dr_0}. \quad (4)$$

All the typical parameters used and the ranges investigated can be found in Table 1 (see Tables S1–S4 for the specific parameters used in each figure). It is worth noting that the three components of our model described above all build on previous experimental observations combined with biophysical results.

Based on this mathematical framework, we first considered the case with only one damaged site, no oscillations in the p53

Table 1. Parameters used in this study with their typical values and the ranges investigated

Parameter	Description	Value	Source	Range	Units
c_{in}	protein concentration inside droplets in the lim $R \rightarrow \infty$	10^6	(Söding et al., 2020)	10^5 – 10^{-7}	μm^{-3}
c_{out}	protein concentration outside droplets in the lim $R \rightarrow \infty$	10^3	(Söding et al., 2020)	$(0.8$ – $1.5) \times 10^3$	μm^{-3}
\bar{c}_0	mean average concentration of proteins in the nucleus	10^3	(Söding et al., 2020)	$(0$ – $3.5) \times 10^3$	μm^{-3}
A_c	amplitude of average concentration in the nucleus	10^2	(Chen et al., 2016)	$(0$ – $8) \times 10^2$	μm^{-3}
ω	frequency of p53/average proteins concentration	0.02	(Geva-Zatorsky et al., 2006)	10^{-3} – 10^1	min^{-1}
l_γ	capillary length	5×10^{-6}	(Söding et al., 2020)	10^{-6} – 10^{-4}	μm
D	diffusion coefficient outside droplets	10	(Matsuda et al., 2008)	1–100	$\mu\text{m}^2\text{s}^{-1}$
D_0	diffusion coefficient inside droplets	0.1	(Miné-Hattab et al., 2021)	0.01–1	$\mu\text{m}^2\text{s}^{-1}$
r_n	radius of the nucleus	5.0	(Sun et al., 2000)	fixed	μm
r_0	radius of the target to repair	0.01	(Heltberg et al., 2021b)	fixed	μm
N	no. of damaged sites	15	(Pessina et al., 2019)	5–50	dimensionless
M	no. of repair steps	40	(Mohseni-Salehi et al., 2020)	40–3,000	dimensionless
λ	rate of damage recreation	0.01	(Hahnfeldt et al., 1992)	0.01–1.5	min^{-1}

See STAR Methods for further explanation on the choices of parameters values and ranges. See Tables S1–S4 for the specific parameters used in each figure.

dynamics and the constant level of $\bar{c} = \bar{c}_0 \forall t$ always above the critical concentration c_{out} (Figure 1I, full line). In this setting, we observed a constant rate of damage repair that is optimized for intermediate values of \bar{c} ($\bar{c}_0 = 1.05c_{out}$) (Figure 1I, dashed line). Indeed, we found that increasing this value too much ($\bar{c}_0 = 2c_{out}$) leads to a reduced decay rate (Figure 1I, dotted line), since the focus grows too large, thus increasing the search time.

On the other hand, in the case of multiple DSBs subject to the Ostwald ripening mechanism, some of them will dissolve, resulting in a significantly inhibited repair rate and an overall repair process that is far from optimal (Figure 1J; note the same color code as the droplets shown in Figures 1D and 1E). This result highlights the problems that the cell encounters with several damaged sites. While the formation of liquid foci can lower the search time of proteins significantly, it has the inherent problem that when multiple sites are present, due to the metastability of the system, small droplets will dissolve before the site is repaired. The next section will discuss how the oscillations found in p53 might influence this situation.

Multiple sites reparation is enhanced by oscillations and suggests the existence of optimal frequencies

In order to investigate the behavior of the system in the presence of p53 oscillations, we first assumed that the p53 concentration can be approximated by a sinusoidal, which would lead to the same dynamics for the average repair proteins concentration:

$$\bar{c} = \bar{c}_0 + A_c \sin(\omega t). \quad (5)$$

Therefore, \bar{c} is calculated at each time step and is then inserted in Equation 2, as mass conservation naturally still holds, in order to determine the value of $c_\infty(t)$. This, in turn, affects the droplet growth through Equation 1. Thereby, the oscillations of the droplet material are mediated through the proteins' concentration far away (c_∞), thus indirectly affecting the foci.

In order to ensure robustness of the model, we tested other simple possible waveforms for p53 (Figure S1A), and non-linear dependencies between p53 and droplet proteins concentration (Figure S1B), still obtaining similar outputs.

By assuming $\bar{c}_0 \geq c_{out}$, one could logically analyze the expected behavior before turning to simulations. If either $A_c = 0$ or $\omega = 0$, the behavior is analogous to the one seen in Figures 1E–1J; on the other hand, as ω becomes similar to the timescale of droplet separation, one droplet would still grow and dominate, but only in the time allowed by the external period. This means that oscillations would effectively prevent Ostwald ripening, thereby allowing the cell to distribute resources among the sites.

To test these predictions, we simulated the typical p53 period of ~ 5 h (Lahav et al., 2004) and observed the formation and dissolution of droplets, with different droplets dominating in different periods (Figure 2A). By combining this dynamics with the damage removal mechanism, we observed that for slow oscillations only one site would be repaired within the simulation time (Figure 2B, left). For the p53 period, the dominating droplets grow to optimal sizes, giving enough time to repair the damaged site properly within each oscillation (Figure 2B, middle). For oscillations much faster than p53, droplets would still emerge, but they would in this regime dissolve well before the sites could be fully repaired (Figure 2B, right). Therefore, this result suggested that optimal frequencies for oscillations could exist. Simulating the system over a wide range of frequencies, we found that the only ones able to achieve a full DNA repair—within a maximum simulation time of 100 h—were those on the timescale of hours (Figure 2C). In those cases of full damage repair, we further recorded the time to reach this condition, which we indicated by a color gradient from blue to red (Figure 2C, see right color bar): *the experimental p53 frequency turned out to be among the most efficient values to repair the damage in the presence of multiple DNA breaks*.

To validate these results, we first simulated the system with several values of damaged sites N, studying whether a high

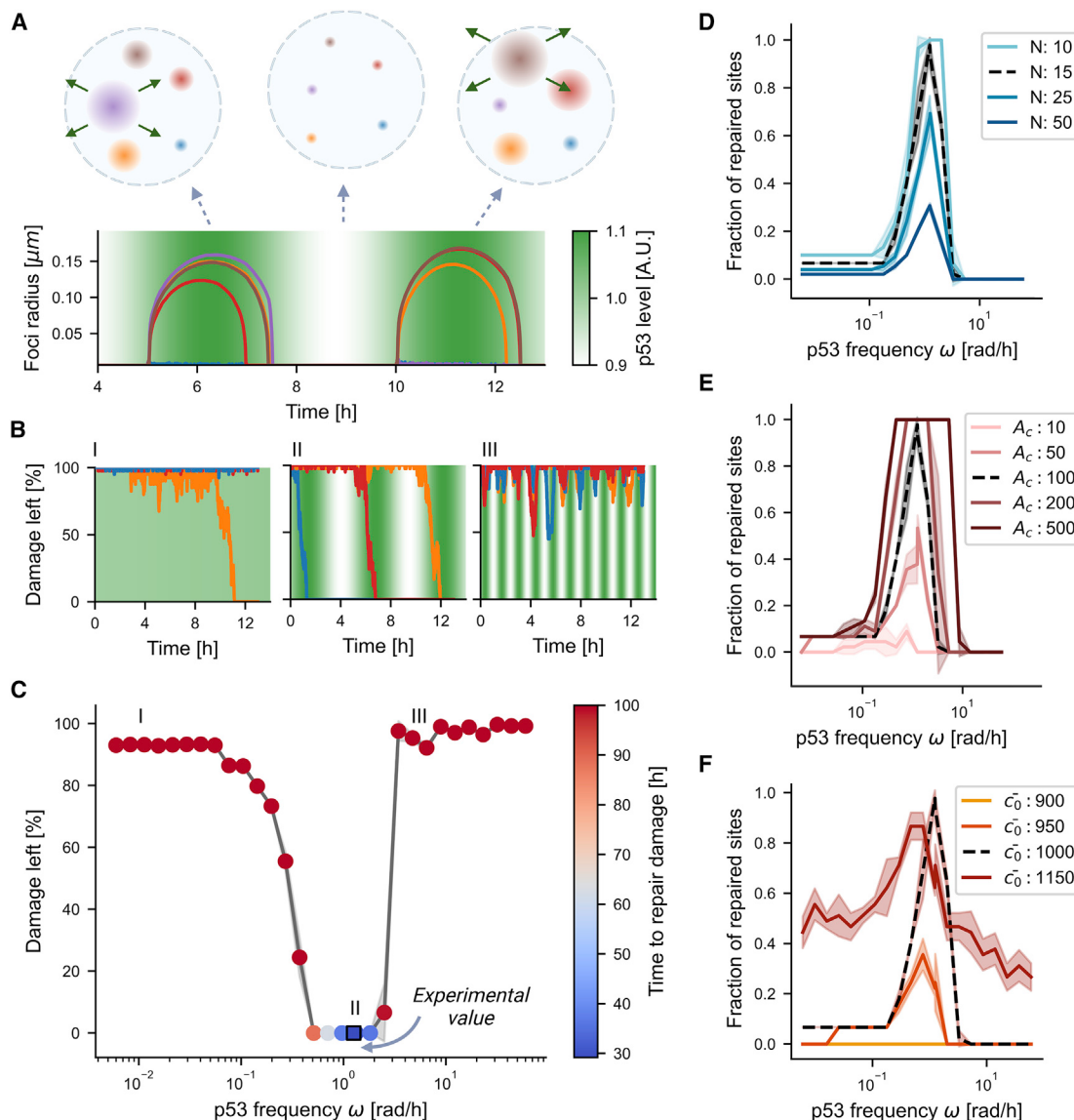


Figure 2. p53 periodicity optimizes the damage repair process in the fast droplets formation regime

- (A) Droplet sizes at various points in time (above) and the radii of five damaged sites (below) in the presence of p53 oscillatory dynamics (green gradient).
 - (B) Damage at each individual site as a function of time (note that, for simplicity, only three traces out of the $N = 15$ are shown here). Left: $\omega = 0.01 \text{ rad h}^{-1}$; middle: $\omega = 2\pi/5.5 \text{ rad h}^{-1}$ (experimental value); right: $\omega = 5 \text{ rad h}^{-1}$.
 - (C) The total amount of damage left on the sites after 100 h as a function of applied frequency. For the sites that were fully repaired, the color bar indicates the time necessary to remove all the damage.
 - (D) Fraction of repaired sites after 30 h as a function of frequency. The four curves represent different initial numbers of damaged sites N , while the shaded area corresponds to the SD. The black dashed curve corresponds to the parameters used in (C) (with the only difference of a shorter simulation time).
 - (E) Same as (D) but shown for five different values of the oscillatory amplitude A_c .
 - (F) Same as (D) but shown for four different values of the mean concentration level \bar{c}_0 . The shaded region in (C)–(F) corresponds to the SD calculated by simulating the system multiple times, and assuming Gaussian errors, dividing by the square root of the number of runs.
- See Table S2 for the specific parameters used in this figure.

competition among numerous sites would prevent the droplets from reaching an optimal radius within the considered periods. On the contrary, we found that the peak in the fraction of repaired sites was conserved over a wide range of N (Figure 2D). Next, we investigated how the result depended on the amplitude and

found that increasing amplitudes enhance the overall repair rate of the system (Figure 2E). Finally, we tested the dependency on \bar{c}_0 , since this had so far only been evaluated at the critical level. What we found is that for low values of \bar{c}_0 , the repair rate is significantly decreased, which is not surprising since the

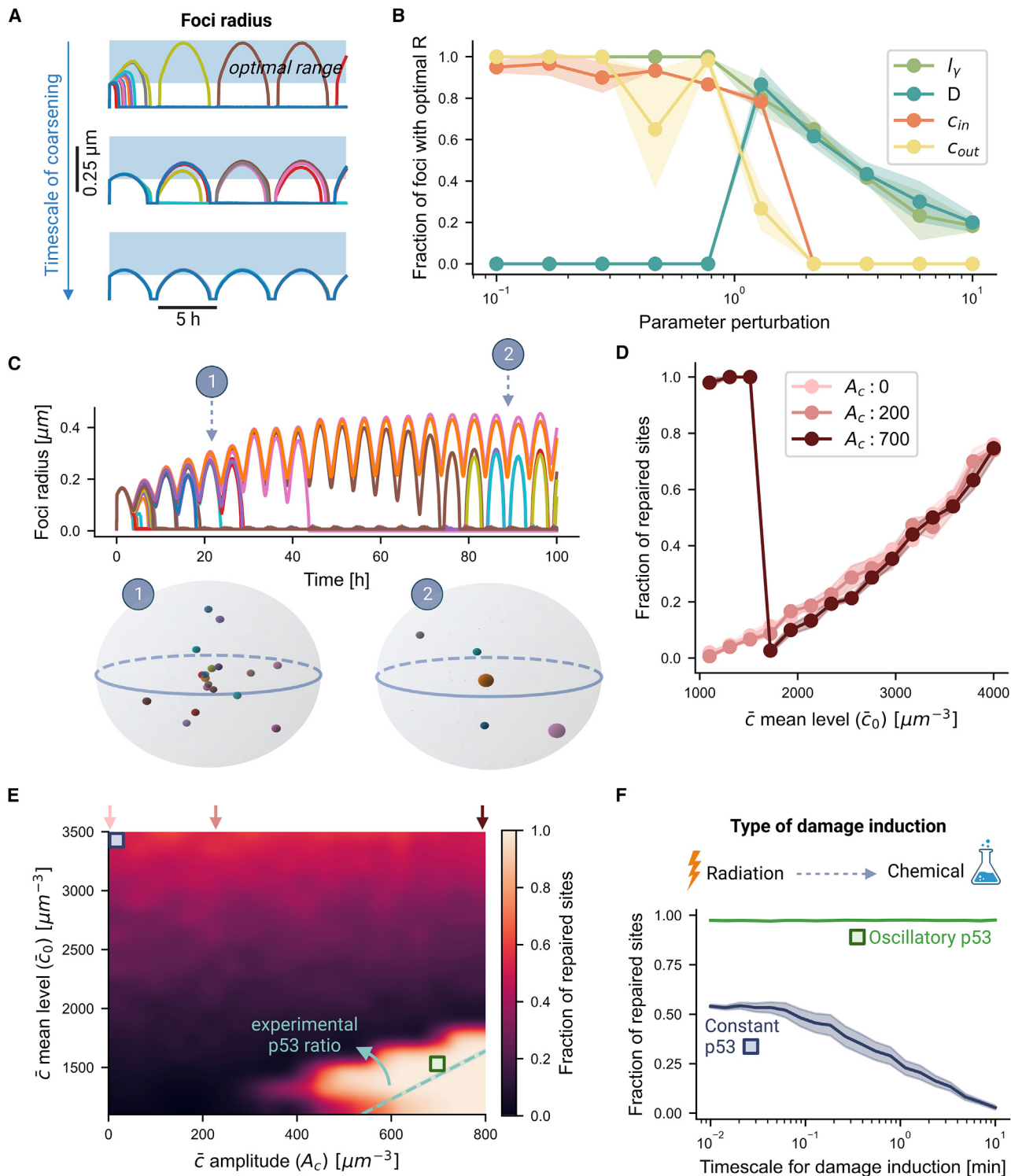


Figure 3. p53 oscillations stabilize droplets sizes in the slow droplets formation regime

(A) Foci radius as a function of time. Three graphs shown for increasing timescales of coarsening (obtained by varying I_Y). The light-blue shaded region indicates the optimal range of radii for which repair of one step of damage takes less than 0.5 min.

(B) Fraction of droplets around a specific site that spend time in the optimal range, for variations in the parameters I_Y , D, c_{in} , and c_{out} . See also Figure S2.

(C) Radii of individual foci as a function of time, when the average concentration is above the critical concentration. Different colors correspond to different foci. Points 1 and 2 (below) visualize the droplet environment at these specific points in time.

(legend continued on next page)

critical concentration spends less time above the critical state; therefore, droplets exist for shorter times. However, by increasing the level of \bar{c}_0 , the repair rate is less sensitive to the frequency, and the maximal repair rate is reduced compared to the critical concentration (Figure 2F). This suggested a fundamental relation between the amplitude of oscillations A_c and the average concentration level \bar{c}_0 .

We speculated that enhancing the average concentration might change the number of stable droplets as more material might be available, thereby enhancing the overall repair rate significantly.

Stabilization and optimization of multiple droplets by enhancing amplitudes

At this stage, our results had revealed how the oscillatory behavior of p53 could distribute the limited resources at the specific damaged sites over time. This naturally brought up the questions (1) what would happen with a wider availability of droplet material, and (2) how would the whole picture be altered in case of a faster/slower droplet coarsening?

To shed light on this, we first considered two factors: in particular, the point when competition for material starts and the point when Ostwald ripening is “complete”—i.e., when one droplet has become dominant. The first occurs when $c_\infty \approx c_{out}$, and following Equation 2, one can derive the formula for the volume of the i -th droplet V_i at which competition for material starts (see STAR Methods),

$$V_i \approx \frac{\bar{c} - c_{out}}{c_{in} - c_{out}} \cdot \frac{V_n}{N} \approx \frac{\bar{c} - c_{out}}{c_{in}} \cdot \frac{V_n}{N}, \quad (6)$$

the last holding since $c_{in} \gg c_{out}$. Consequently, we derived the timescale of Ostwald ripening (T_{OR}), that is the time necessary for one droplet to dominate on the others (Söding et al., 2020) (see STAR Methods), which takes the form

$$T_{OR}(R) = \frac{R_c}{Dl_\gamma} \frac{c_{in}}{c_{out}} R^2, \quad (7)$$

where R_c is the critical radius for the system in steady state. If the timescale of coarsening is lower than the period of p53 oscillations, the dominating droplet quickly prevails within each period, preventing all the others from growing (Figure 3A, top). On the other hand, for longer T_{OR} , multiple droplets, with volume given by Equation 6, may co-exist within each oscillation (Figure 3A, bottom) as Ostwald ripening (and competition for material) would occur at a much later time. The latter would seem like the optimal scenario for the cell, which would be able to repair multiple sites simultaneously within each period. It should be noted, though,

that in this case the maximum radius reached by the droplets is lower than before, as material is distributed equally among all of them. Following this reasoning, we defined an “optimal range” of radii (light-blue shaded region of Figure 3A) around the minimum of τ (Equation 3), where damage repair would be the fastest and chose an interval such that one damage removal would take less than 0.5 min. At this point it was clear that a slower timescale of coarsening would benefit the cell only in the presence of enough material to distribute among the foci, in order to perform a parallel repair of multiple damaged sites.

Following Equation 7, we then investigated the role of the different parameters ($D, c_{in}, l_\gamma, c_{out}$) in altering the timescale of coarsening and consequently the number of droplets whose radius is within the optimal range (Figure 3B). We found that increasing l_γ leads to a shorter timescale of coarsening and therefore a lower number of droplets whose size is in the optimal range. Increasing the diffusion coefficient D both results in a fast timescale of coarsening but also in a wider range of optimal radii. On the other hand, greater c_{in} results in progressively smaller droplets that do not grow in the optimal range. Finally, we realized that varying c_{out} over two orders of magnitude, such that the system transitions from being constantly supersaturated ($c_{out} < \bar{c}$) to undersaturated ($c_{out} > \bar{c}$) leads to stabilization of droplets in the first case and impossibility to grow in the latter (see Figure S2 for explanatory panels).

Next, we further investigated what would happen if the mean concentration were significantly increased, such that oscillations of \bar{c} would always be above the critical concentration c_{out} . In this case the system revealed an interesting property: while Ostwald ripening still occurs in the sense that one droplet dominates in the end (Figure 3C, point 2), the meta-stable state can exist for a very long time (Figure 3C, point 1), and many of the otherwise dissolved sites still show droplets emerging. However, in this picture the Ostwald ripening also results in a vast amount of material centered around a few number of sites until only one dominates.

Therefore, we wondered how the number of repaired sites would scale as the mean concentration were elevated. We found that in the absence of oscillations, there is a linear relation between the number of repaired sites and the mean concentration (Figure 3D, pink curve). The reason is that increasing the amount of material leads to more states that can co-exist in the meta-stable state before they dissolve, resulting in more repaired sites. However, introducing oscillations and increasing the amplitude, we observed a new region emerging, where the damage is resolved at a much higher rate (Figure 3D, brown curve). In this regime the effect of the oscillations is large enough to prevent the Ostwald ripening, while there is still enough material available for droplets to grow to optimal sizes. This suggested a non-trivial relation between the average concentration and the values of the

(D) Fraction of fully repaired sites as a function of the mean concentration level. Curves are shown for three different values of the amplitude.

(E) Heatmap showing the fraction of repaired sites (indicated by colormap) as a function of the amplitude (x axis) and the mean concentration level (y axis). The three small arrows on the top correspond to the three values of A_c investigated in (D). The light-blue dashed line represents the experimental p53 ratio between the average p53 level and its amplitude. The green and blue squares show the parameters used in (F).

(F) Fraction of repaired sites assuming different timescales for damage induction, spanning from fast (radiation induced) to slow (chemically induced); oscillatory p53 (green line) is always advantageous against constant p53 level (blue line). The shaded region in (B), (D), and (F) corresponds to the SD calculated by simulating the system multiple times, and assuming Gaussian errors, dividing by the square root of the number of runs.

See Table S3 for the specific parameters used in this figure.

amplitude, and we realized that a region of optimal DNA repair emerged for large values of the amplitude and intermediate values of the mean concentration (Figure 3E). Moreover, we quantified the ratio r between mean level and amplitude in the experimental p53 signal (Figure 1B), obtaining $r = 2.050 \pm 0.023$. Very interestingly, by plotting the line with slope corresponding to r , we discovered that it spans precisely the region of optimal repair (light-blue dashed line, Figure 3E).

Up to now, we have considered an instantaneous initial nucleation (corresponding to irradiation), but in nature damage might often be chemically induced reflected by a longer timescale, and thereby higher variation, in the initial nucleation time. We observed that for a large time of damage induction, some initially larger droplets quickly take up all material, leading to non-optimal repair (Figure 3F, blue line). This does not affect the droplets in the presence of p53 oscillations (Figure 3F, green line), which ensure the distribution of material to different sites over time.

This aspect highlights the overall advantageous effect of p53 oscillations compared to constant levels.

Enhancing the repair by parameter stimulation and noise induction in the p53 network

Finally, we combined the theory of droplets with the p53-Mdm2 protein network, in order to make predictions on how altering this network, with stochastic noise, affects the DNA repair. The network of p53 takes the form (Mengel et al., 2010):

$$\begin{aligned} \frac{dp}{dt} &= k_1 - k_2 M \frac{p}{k_3 + p} \\ \frac{dm}{dt} &= k_4 p^2 - k_5 m \\ \frac{dM}{dt} &= k_6 m - k_7 M \end{aligned} \quad (8)$$

where p , m , and M are the concentration of p53, of Mdm2-mRNA, and Mdm2 itself, respectively. In this model, the material forming droplets still follow p53 concentration linearly, and p53 is produced at a fixed rate (k_1) and degraded following binding to Mdm2 by a saturated degradation process (k_2, k_3). The Mdm2-mRNA is produced proportionally to the p53 level squared—since p53 acts as a dimer—scaling with a production parameter (k_4) and degraded through a first-order decay process (k_5). Finally, the protein Mdm2 is produced proportionally to the Mdm2-mRNA with constant k_6 and again degraded through a first-order decay process (k_7). Inspired by previous analyses, we used simulations to make the network agree with the biological findings, where p53 levels are constant until stimulated externally, at which point oscillations arise with a frequency of ~ 5.5 h (Figure 4A).

In order to include stochasticity, we simulated the model using the Gillespie algorithm (see STAR Methods), which let us combine the dynamics of p53 with the dynamics of droplet formation and damage removal. We first analyzed the behavior of the limit cycle by varying the parameters with particular interest in the role of enhanced degradation (k_2), since we have previously revealed that this is a main component in the induction of

p53 oscillations (Heltberg et al., 2019a). We found that high values of k_2 result in low, non-oscillatory, steady-state levels of both p53 and Mdm2. On the other hand, decreasing k_2 gives rise to a Hopf-bifurcation and a stable limit cycle, but very low levels of this parameter again lead to a non-oscillatory state, regardless of the p53 and Mdm2 levels. We visualized this by plotting the levels of p53 versus the level of Mdm2 after the transient phase, where the dynamics had reached the steady state. In the phase spanned by their concentrations, we observed how the limit cycle can emerge for intermediate values of k_2 (Figure 4B, top). The same behavior can be obtained by increasing the Mdm2 production rate k_4 , whereas increasing the p53 production by enhancement of k_1 mainly results in a continuous increase in the amplitude of p53 (Figure 4B, bottom). See Figure S3 for the correspondent time series. Based on these considerations, we investigated the repair rate by perturbing the three parameters, k_1 , k_2 , and k_4 (Figure 4C). The regions of optimal repair were those corresponding to high amplitudes and optimal mean levels for the p53 signals, obtained for intermediate values of k_2 and k_4 (red and purple curves) and high values of k_1 (yellow curve).

Finally, we investigated the role of noise in the p53 oscillations on the droplet formation and repair rate (Figure 4D). Visualizing the p53-Mdm2 trajectories in polar coordinates (see STAR Methods) reveals that higher noise levels amplify the SD, pushing the radial coordinate outward and therefore leading to effectively enhanced amplitudes (Figure 4E).

Based on these observations, we hypothesized that stochasticity in the oscillator could be a method to further enhance the repair rate, and we found that this is particularly effective for situations with many damaged sites (Figure 4F). Thereby, we concluded that the protein network could be tweaked to optimize the repair rate both through adjusting the parameters and enhancing the stochasticity.

This theoretical work overall reveals how the dynamics of oscillations can be used in saturated environments, to distribute resources over nucleation points in time and space. This in turn not only prevents the Ostwald ripening from introducing a monopoly on resources for one large droplet but also enables a few droplets of optimal size to exist instead, thereby optimizing the use of material. In Figure 4G, we have schematically summarized these conclusions into a working model that might stimulate future research in the combination of dynamics and phase transitions. Based on this, we wanted to experimentally test the most striking feature of our conclusions: that the oscillatory dynamics in p53 would enhance the efficiency of DNA repair.

Model's predictions and their validation

Our theoretical model directly leads to predictions that can be experimentally tested (Figure 5A). Since the mechanism proposed is quite delicate, depending on the quantitative nature of the biological oscillators (e.g., period, amplitude), we believe it should be tested in multiple cell lines, possibly including non-cancerous ones. Indeed, the fine balance of phase transitions and the ability to form and dissolve repair foci could easily be disturbed or suppressed in a cell-line- and context-dependent manner.

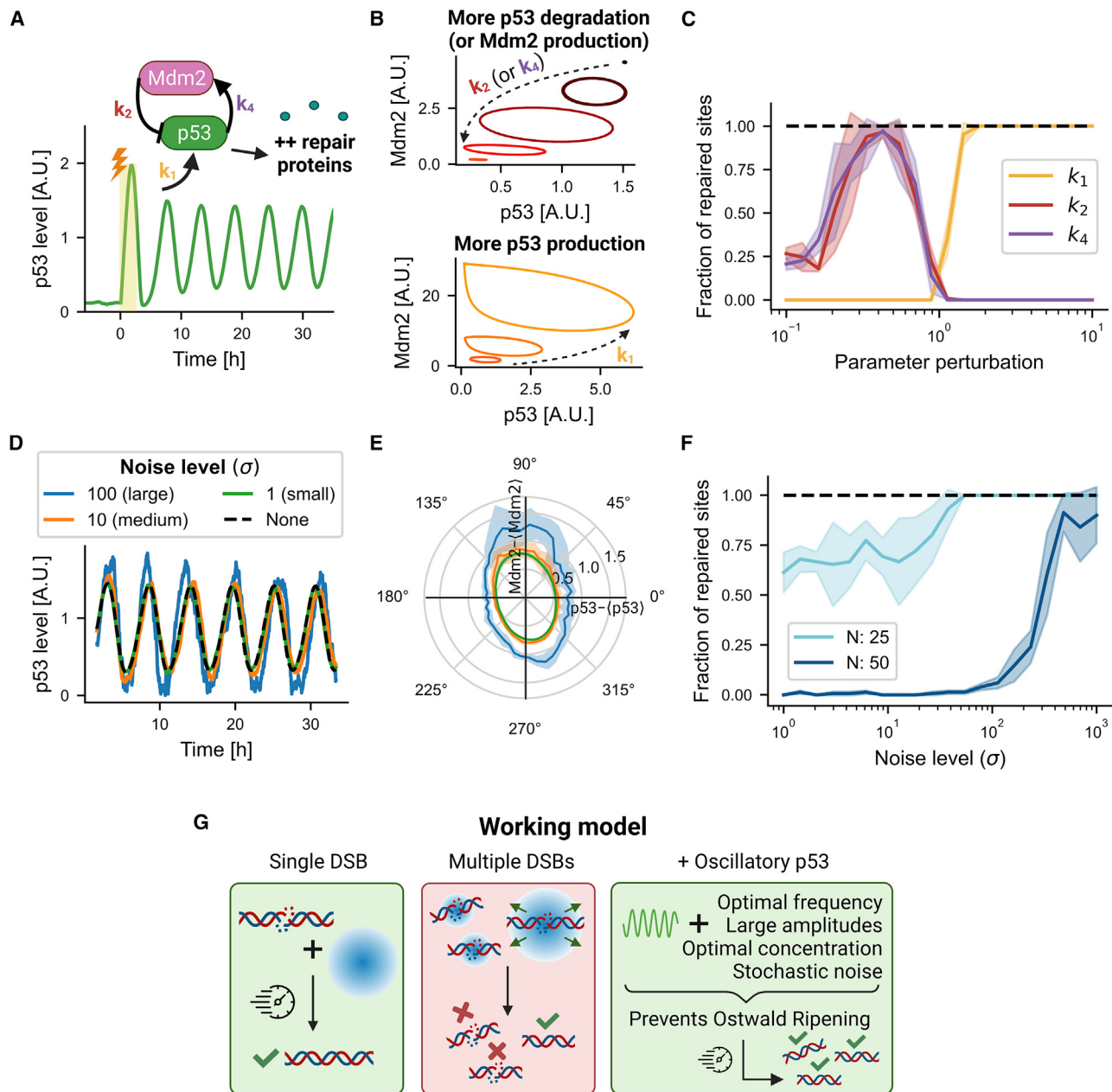


Figure 4. Tweaking p53 network parameters and enhancing the stochasticity may optimize the repair rate

(A) Simulated trace of p53 according to the model of Equation 8, following induction of damaged sites.

(B) Visualization of the steady-state phase space, spanned by p53 and Mdm2, for different parameter choices. Top: increased p53 degradation, thus higher k_2 . Note that increased Mdm2 production (i.e., higher k_4) leads to the same behavior (not shown). Bottom: increased p53 production, thus higher k_1 . See also Figure S3.

(C) Fraction of repaired sites, as a function of parameter perturbations in the parameters k_1 , k_2 , and k_4 . Shaded areas correspond to the SD on these numbers.

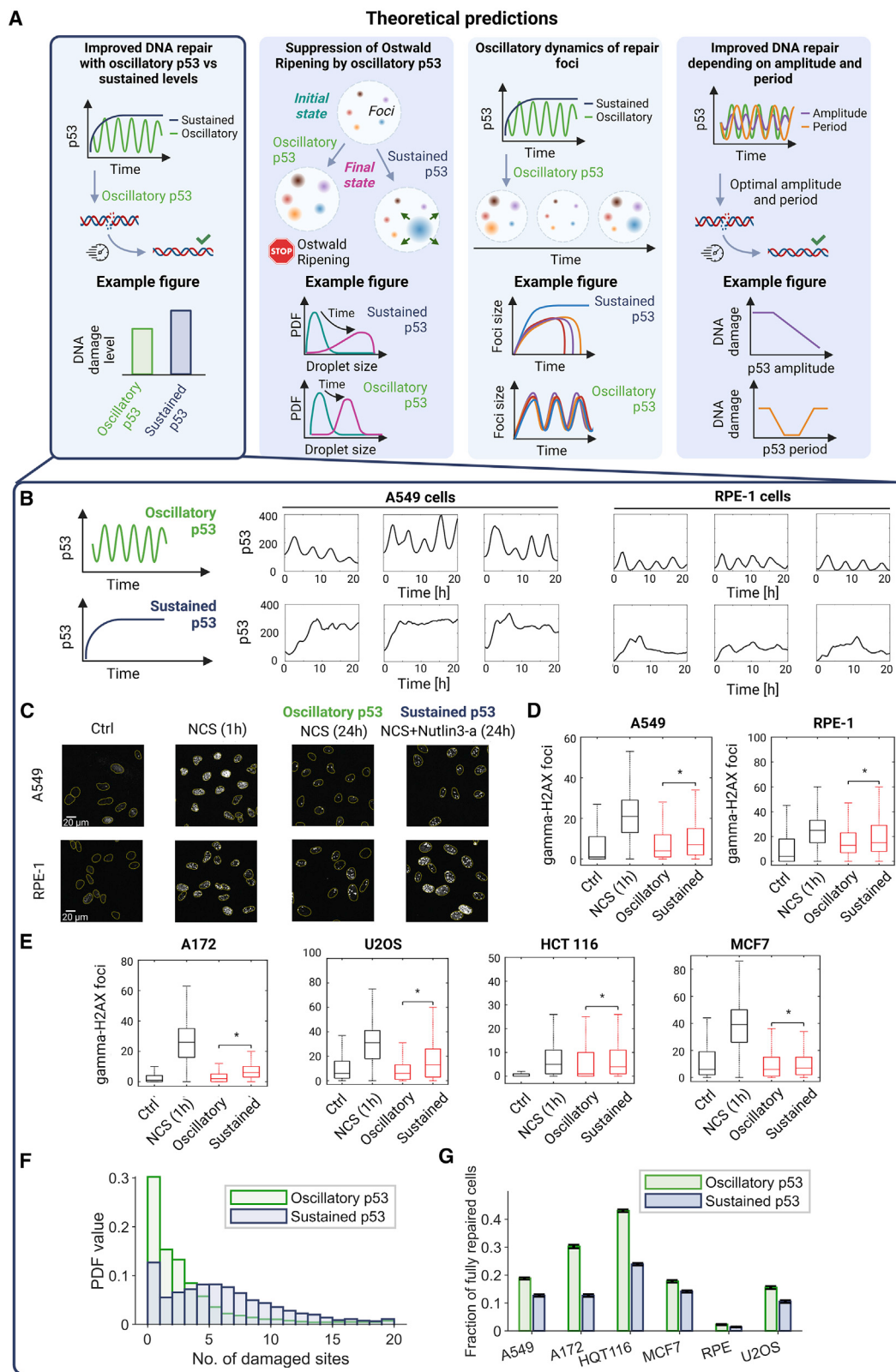
(D) Nuclear concentration of p53 as a function of time, shown for three different levels of noise and the related deterministic simulation.

(E) The p53-Mdm2 phase space transformed into polar coordinates, shown for the three levels of noise. In both (D) and (E), noise was introduced by applying the Gillespie algorithm.

(F) Fraction of fully repaired sites as a function of the applied noise level in the external concentration oscillations. Two curves shown for different numbers of initially induced damaged sites. Shaded areas correspond to the SD on these numbers.

(G) Schematic figure, revealing the working model of how a single damaged site can be repaired fast and efficiently through the formation of a droplet and how multiple damaged sites need external dynamics to prevent Ostwald ripening and maintain this functioning role.

See Table S4 for the specific parameters used in this figure.



(legend on next page)

The first of our predictions is that the p53 oscillations should be more efficient in repairing DNA damage compared to sustained levels, leading to a higher number of fully repaired sites. This can be experimentally tested by controlling the p53 dynamics—oscillatory vs. sustained—and by measuring in each case the DNA damage level, as shown in an “example figure” in Figure 5A, left.

Second, we predict that the oscillations in p53 can prevent the coarsening of DNA repair foci and thereby prevent some droplets from growing to extreme sizes. This could be tested by measuring the size distribution of DNA repair foci at different time points, similar to Pessina et al. (2019)—the authors there used U2OS cells, whose p53 dynamics is highly sensitive to the level of genotoxic stress and is dose dependent (Stewart-Ornstein and Lahav, 2017; Yang et al., 2018); therefore, it is likely not oscillatory under their conditions (2 Gy). Due to Ostwald ripening, the foci would grow to larger sizes in case of sustained p53 levels (Figure 5A, bottom mid-left). To monitor the coarsening of the DNA damage foci, there are two candidate markers, 53BP1 (Pessina et al., 2019) and MRNIP (Wang et al., 2022b). Distinct in their function, 53BP1 and MRNIP represent the DNA damage repair foci via the mechanisms of non-homologous end-joining (NHEJ) and homologous recombination (HR), respectively. These markers can be introduced to a p53 reporter cell line for simultaneous quantification of p53 and DNA damage foci dynamics.

Third, our prediction is that the DNA repair foci, in the presence of p53 oscillations, should show some kind of oscillatory dynamics too. This also means that those repair foci that would disappear under sustained p53 levels, due to Ostwald ripening, should instead be maintained under p53 oscillations. We suggest that this hypothesis could be tested by measuring the dynamics of DNA repair foci in their number and intensity over time (Figure 5A, bottom mid-right).

Finally, our model predicts that p53 may have some optimal amplitude and frequency to perform DNA repair. We suggest to test this aspect by altering the properties of p53 oscillations while quantifying the DNA repair efficiency (Figure 5A, bottom right). Since our predicted valley in Figure 2C is relatively broad, we suspect that one would need to change the frequency of p53 oscillations by an order of magnitude in order to observe significantly altered results. In contrast, the amplification of the amplitude should lead to an obvious improvement of the DNA repair efficiency.

We therefore sought to experimentally test the most fundamental hypothesis: the oscillatory p53 dynamics promotes DNA repair efficiency. Therefore, we introduced DNA damage by adding neocarzinostatin (NCS), a γ -irradiation mimetic drug that causes DSBs and oscillatory p53 dynamics (Figure 5B, top). In order to achieve sustained p53 dynamics, we added a non-genotoxic small molecule, nutlin-3a, that stabilizes p53 by suppressing its Mdm2-mediated ubiquitination and degradation. Nutlin-3a was added 2.5 and 5.5 h after NCS treatment to obtain sustained p53 dynamics in A549 and RPE-1 cells (Figure 5B, bottom). We then quantified the DNA damage levels by immunofluorescent staining of the γ -H2AX foci before and 1 h after DNA damage, as well as 24 h after DNA damage introduction under the oscillatory or sustained p53 dynamics (Figure 5C). Note that these DNA damage foci are different from the DNA repair foci (e.g., ones measured in Pessina et al. [2019]) as they have not been shown to exhibit liquid-droplet properties and are merely representing the levels of DNA damage. Based on the immunofluorescent images, we quantified the number of γ -H2AX DNA damage foci in individual cells. Figure 5D shows that cells with oscillatory p53 dynamics have a lower number of γ -H2AX foci 24 h after NCS treatment, thus exhibiting higher DNA damage repair efficiency, compared to those with sustained p53.

To further strengthen these observations, we carried out the same experiments in four more cell lines: A172, U2OS, HCT116, and MCF7. Interestingly, in all of them, cells with oscillatory p53 dynamics show less γ -H2AX DNA damage foci 24 h after DNA damage compared to those with sustained p53 (Figure 5E), supporting the prediction of oscillatory p53 in promoting DNA damage repair. To further validate that the distributions of damage differed between cells with oscillatory p53 and sustained levels, we performed a two-sided KS test and obtained p values smaller than 10^{-7} . Finally, we also investigated the fraction of cells that were completely repaired, which is often the most significant value in biology. Here, we found that all cell lines with oscillatory p53 had a larger fraction of fully repaired cells, and calculating the probability that the oscillatory cell lines would have more fully repaired cells, we obtained p values smaller than 10^{-6} for all cell lines (see Figures 5F and 5G).

Taken together, our experimental results are in strong agreement with the first theoretical prediction and reveal that the oscillations in p53 can enhance the efficiency of DNA repair.

Figure 5. Model-inspired hypotheses and experimental validation

- (A) Schematics showing four theoretical predictions and suggested example figures for validation through experimental measurements.
(B-E) Experimental results testing the leftmost (encircled) hypothesis.
(B) p53 oscillatory (top) and sustained (bottom) dynamics in three representative A549 (left) and RPE-1 cells (right).
(C) Immunofluorescent images of γ -H2AX DNA damage foci under oscillatory and sustained p53 dynamics. DNA damage was introduced by treating cells with NCS (400 ng/ml). Upper: A549 cells; lower: RPE-1 cells. First column: control before introducing DNA damage; second column: 1 h after DNA damage introduction by addition of NCS; third column: 24 h after DNA damage introduction under oscillatory p53 dynamics (NCS treatment alone); fourth column: 24 h after DNA damage introduction in the presence of sustained p53 levels (NCS + nutlin-3a, see STAR Methods for details).
(D) Quantification of γ -H2AX DNA damage foci in A549 (left) and RPE-1 cells (right). γ -H2AX foci under oscillatory and sustained p53 dynamics were labeled in red ($n > 1,000$, Wilcoxon rank-sum tests, $*p < 10^{-19}$).
(E) Quantification of γ -H2AX DNA damage foci in four additional cell lines. From left to right: A172, U2OS, HCT116, and MCF7 ($n > 1,000$, Wilcoxon rank-sum tests, $*p < 10^{-9}$).
(F) Distribution of the number of damaged sites in cells. Data shown for A172 cell line.
(G) Barplot showing the fraction of fully repaired sites and the uncertainty on this number.

DISCUSSION

How oscillations in TFs can be used to optimize specific processes and why evolution has created these complex responses remain open and deep questions. The emerging evidence that DNA repair foci might form as a result of liquid–liquid phase separation, inspired us to investigate the interplay between oscillations in TFs, such as p53, and the formation of multiple droplets. We thus revealed that the properties of oscillations can stabilize these structures in an ordered and efficient way, leading to an optimal repair mechanism.

These two aspects had not been combined in areas of biophysics before. Hereby, we do not only show an interesting result based on coupled differential equations but apply a direct biophysical mechanism that mediates the connection and creates the optimal repair strategy, offering clear experimentally testable predictions. The vast majority of parameters applied in this work are well defined from numerous experiments, and even though some values can differ (the number of damaged sites and the concentration inside droplets), our results are robust to variations in these parameters and overall suggest why oscillations can be of fundamental importance.

Droplet formation is a popular topic in science, and many experiments have currently reported the observation of liquid sub-compartments in the cell (Brangwynne et al., 2009; Larson et al., 2017; Strom et al., 2017). Preventing the Ostwald ripening has been the topic of many papers, who sought to create a stationary state in the equation for droplet growth and thereby to chemically stabilize droplet sizes. The mechanism that liquid droplets can oscillate in size, thereby preventing Ostwald ripening, has been shown to occur for nanoparticles (Xin and Zheng, 2012), but other ways to stabilize the droplets have also been suggested. One mechanism, for instance, consists in the inclusion of trapped species in the dense phase (Webster and Cates, 2001), where droplets will grow to a specific (relatively small) size, unless they cross a critical threshold where the large droplets will again grow. Another possibility is to considerably slow down Ostwald ripening—which for normal timescales might be enough to stabilize the emulsions—by lowering the surface tension so that it becomes effectively zero. Moreover, the chemical turnover of droplet material inside the droplet has been recently indicated as another way to obtain a stationary state (Söding et al., 2020; Weber et al., 2019; Zwicker et al., 2015; Kirschbaum and Zwicker, 2021). However, if the droplet material is finite and many damaged sites emerge, preventing Ostwald ripening altogether might not be optimal, since the remaining droplets will then share the material and all be small. With oscillations, in the presence of Ostwald ripening, material can be clustered at some specific sites, only to be redistributed at later times at other sites. We speculate that this might further optimize processes in biology, where material needs to be shared among a variable number of locations.

In this work we focused on how downstream repair is stimulated by p53. We assume for simplicity that the proteins causing the phase transition are stimulated as a linear function of the p53 concentration. Present literature has revealed that p53 not only works as a TF for the proteins related to DNA repair but also directly recruits important proteins such as 53BP1 and DDP1,

whose concentrations seem to scale linearly with the p53 level (Wang et al., 2022a). Moreover, it has been shown that p53 is one of the fastest proteins to relocate to the site of DNA damage, which occurs on timescales of seconds (Wang et al., 2022a), whereas studies *in vitro* have found that p53 itself can form a liquid droplet state (Kamagata et al., 2020; Petronilho et al., 2021). These results may suggest that p53 plays a crucial role on shorter timescales and on a more direct level than what is typically considered as a downstream effect, being a potential main candidate to induce the droplet formation observed in DNA repair. On the other hand, we have shown (Figure S1B) that a non-linear relation between p53 and downstream droplet proteins anyway results in the majority of cases in an oscillatory signal for the droplet proteins concentration.

At the same time, the oscillations in p53 could very well be stimulated themselves by the damaged sites and thereby possibly by the intensity of foci. This could potentially be a sensing mechanism that signals back to the p53 loop and stops it from oscillating when all sites have been successfully repaired. Furthermore, it is well known that cells showing oscillations in the p53 concentration can become senescent after some time, which could again be an interesting signal from the foci structures. We thus hypothesize that the present results are one link in the network that couples p53 dynamics, DNA repair, and ultimately cell-fate decisions.

In this regard, it is also interesting to consider that p53 has been revealed to show circadian oscillations, through the interaction with circadian protein Per2 (Gotoh et al., 2015, 2016). However, these oscillations occur in the absence of multiple damaged sites, which is the main problem investigated in this paper. Nevertheless, if the oscillations of p53 due to DNA damage interfered with the circadian oscillations, there could be an intriguing interplay. Indeed, this would theoretically constitute a set of coupled oscillators, where one could imagine that the periodicity of the damage-related oscillations could entrain to the external, circadian oscillator.

The reparation of damaged sites is a complicated process involving a large number of steps and specific proteins that we mathematically modeled and approximated as a discrete Markov chain. It is important to note that the actual structure of such a chain is not crucial to the results. Indeed, it merely represents the feature of the repair process of having a characteristic time to finish and potentially also the situation where fractionally repaired damaged sites might lose their state if not repaired fully within a characteristic time.

In this work we revealed how oscillations can play an important role both through the amplitude and the periodicity, suggesting that no other type of dynamics (random fluctuations, stability, or chaos) would perform as well, and we validated these theoretical predictions with an experimental verification of the positive role of p53 oscillations on DNA repair. Of course, it is very plausible that the proposed mechanism may work together with other mechanisms in the stabilization of foci and optimization of repair, meaning that the oscillations are only one part of the entire puzzle. Furthermore, there are many other systems with oscillations, for instance in the TF NF- κ B. With the growing evidence that liquid sub-compartments exist in many aspects of cell regulation (Brangwynne et al., 2009; Larson et al., 2017;

Strom et al., 2017), we speculate that these findings might also be fundamental to other aspects of gene regulation in the presence of complex dynamics. If these results really revealed one key role for the oscillations in p53, it would be a major step forward in our understanding of damage repair. It is at least tempting that two fundamental processes in physics might guard one of life's most fundamental regulatory processes.

Limitations of the study

This study presents a theoretical description of droplet formation in an oscillatory field and relates it to the process of DNA repair. Here, we describe the simplified scenario of a binary phase separation along with identical repair proteins. Future research should investigate the properties of this in more complex phase separations and in the presence of active emulsions that might further stabilize the droplets. Furthermore, while the liquid nature of the repair foci has been well established, it is of fundamental importance to reveal which proteins are responsible for creating this phase transition *in vivo*. While we have successfully obtained one experimental validation of the hypotheses of the model, our work is fundamentally of theoretical character, and it needs to be thoroughly tested *in vivo* under many different conditions. The main foundations of the work are (1) DNA repair happens in the presence of droplet formation and (2) p53 stimulates numerous DNA repair processes and shows sustained oscillations following severe degree of DNA damage. These are both well established from experiments, but future experimental work should test whether p53 mediates the phase transitions (either directly by causing the phase separation or indirectly by upregulating proteins responsible for the phase separation) and whether the repair foci can show signs of oscillatory dynamics. We also acknowledge that the experimental results presented in this paper might not produce complete evidence of the specific theoretical mechanisms proposed, and further validation is still needed to reveal the important roles of p53 oscillations.

STAR★METHODS

Detailed methods are provided in the online version of this paper and include the following:

- KEY RESOURCES TABLE
- RESOURCE AVAILABILITY
 - Lead contact
 - Materials availability
 - Data and code availability
- EXPERIMENTAL MODEL AND SUBJECT DETAILS
 - Cell culture
- METHOD DETAILS
 - Live cell imaging
 - Single cell tracking and p53 level quantification
 - Immunofluorescence
 - γ-H2AX foci quantification
 - Parameter estimates
 - First passage time in the Smoluchowski limit
 - Derivation of droplet growth
 - Simulation of droplet growth and damage repair with the Gillespie algorithm

- Transition from diffusion to Ostwald ripening
- Ostwald Ripening timescale of coarsening
- Visualizing p53 dynamics in polar coordinates
- On non-linear p53 stimulation and the dependency of waveforms

● QUANTIFICATION AND STATISTICAL ANALYSIS

SUPPLEMENTAL INFORMATION

Supplemental information can be found online at <https://doi.org/10.1016/j.cell.2022.10.004>.

ACKNOWLEDGMENTS

We are grateful to Galit Lahav, Michael Tsabar, Yonatan Chemla, Judith Miné-Hattab, Angela Taddei, Aleksandra Walczak, and Thierry Mora for inspiration in the work on DNA repair, p53 dynamics, focus formation, and first passage times. We thank Chia-Chou Wu in the Lab for Cell Dynamics for his help with image analysis. This project has received funding from the European Research Council (ERC) under the European Union's Horizon 2020 research and innovation program under grant agreement no. 740704. S.H.C. acknowledges the funding supports from the Taiwan National Science and Technology Council (grant: 111-2311-B-001-012) and from Academia Sinica (grant: AS-CDA-108-L01). M.S.H. acknowledges the Carlsberg Foundation (grant: CF20-0621) and the Lundbeck Foundation (grant: R347-2020-2250). M.H.J. acknowledges support from the Independent Research Fund Denmark (grant: 9040-00116B) and from the Novo Nordisk Foundation (grant: NNF20OC0064978). Figures 1–5 were created with BioRender.com.

AUTHOR CONTRIBUTIONS

Planning and conceptualization, M.S.H. and M.H.J.; Simulations and mathematical analysis, M.S.H. and A.L.; Experimental design, F.-S.H. and S.-h.C.; Carrying out the experiments, F.-S.H.; Analysis of the experimental results, D.P.M.N. and S.-h.C.; Writing the manuscript, M.S.H., A.L., S.-h.C., and M.H.J.; Editing the manuscript, M.S.H., A.L., S.-h.C., and M.H.J.

DECLARATION OF INTERESTS

The authors declare no conflict of interests.

INCLUSION AND DIVERSITY

We support inclusive, diverse, and equitable conduct of research.

Received: April 13, 2022

Revised: August 23, 2022

Accepted: October 5, 2022

Published: November 10, 2022

REFERENCES

- Batchelor, E., Mock, C.S., Bhan, I., Loewer, A., and Lahav, G. (2008). Recurrent initiation: a mechanism for triggering p53 pulses in response to DNA damage. *Mol. Cell.* 30, 277–289. <https://doi.org/10.1016/j.molcel.2008.03.016>.
- Brangwynne, C.P., Eckmann, C.R., Courson, D.S., Rybarska, A., Hoege, C., Gharakhani, J., Jülicher, F., and Hyman, A.A. (2009). Germline P Granules Are Liquid Droplets That Localize by Controlled Dissolution/Condensation. *Science* 324, 1729–1732. <https://doi.org/10.1126/science.1172046>.
- Chen, S.-h., Forrester, W., and Lahav, G. (2016). Schedule-dependent interaction between anticancer treatments. *Science* 351, 1204–1208. <https://doi.org/10.1126/science.aac5610>.
- Gaglia, G., Guan, Y., Shah, J.V., and Lahav, G. (2013). Activation and control of p53 tetramerization in individual living cells. *Proc. Natl. Acad. Sci. USA* 110, 15497–15501. <https://doi.org/10.1073/pnas.1311126110>.

- Geva-Zatorsky, N., Rosenfeld, N., Itzkovitz, S., Milo, R., Sigal, A., Dekel, E., Yarnitzky, T., Liron, Y., Polak, P., Lahav, G., and Alon, U. (2006). Oscillations and variability in the p53 system. *Mol. Syst. Biol.* 2. 2006.0033. <https://doi.org/10.1038/msb4100068>.
- Gotoh, T., Kim, J.K., Liu, J., Vila-Caballer, M., Stauffer, P.E., Tyson, J.J., and Finkelstein, C.V. (2016). Model-driven experimental approach reveals the complex regulatory distribution of p53 by the circadian factor Period 2. *Proc. Natl. Acad. Sci. USA* 113, 13516–13521. <https://doi.org/10.1073/pnas.1607984113>.
- Gotoh, T., Vila-Caballer, M., Liu, J., Schiffhauer, S., and Finkelstein, C.V. (2015). Association of the circadian factor Period 2 to p53 influences p53's function in DNA-damage signaling. *Mol. Biol. Cell* 26, 359–372. <https://doi.org/10.1091/mbc.e14-05-0994>.
- Hahnfeldt, P., Sachse, R.K., and Hlatky, L.R. (1992). Evolution of DNA damage in irradiated cells. *J. Math. Biol.* 30, 493–511. <https://doi.org/10.1007/bf00160533>.
- Heltberg, M., Kellogg, R.A., Krishna, S., Tay, S., and Jensen, M.H. (2016). Noise Induces Hopping between NF- κ B Entrainment Modes. *Cell Syst.* 3, 532–539.e3. <https://doi.org/10.1016/j.cels.2016.11.014>.
- Heltberg, M.L., Chen, S.-H., Jiménez, A., Jambhekar, A., Jensen, M.H., and Lahav, G. (2019a). Inferring Leading Interactions in the p53/Mdm2/Mdmx Circuit through Live-Cell Imaging and Modeling. *Cell Syst.* 9, 548–558.e5. <https://doi.org/10.1016/j.cels.2019.10.010>.
- Heltberg, M.L., Krishna, S., and Jensen, M.H. (2019b). On chaotic dynamics in transcription factors and the associated effects in differential gene regulation. *Nat. Commun.* 10, 71. <https://doi.org/10.1038/s41467-018-07932-1>.
- Heltberg, M.L., Krishna, S., Kadanoff, L.P., and Jensen, M.H. (2021a). A tale of two rhythms: Locked clocks and chaos in biology. *Cell Syst.* 12, 291–303. <https://doi.org/10.1016/j.cels.2021.03.003>.
- Heltberg, M.L., Miné-Hattab, J., Taddei, A., Walczak, A.M., and Mora, T. (2021b). Physical observables to determine the nature of membrane-less cellular sub-compartments. *Elife* 10, e69181. <https://doi.org/10.7554/elife.69181>.
- Hoffmann, A., Levchenko, A., Scott, M.L., and Baltimore, D. (2002). The I κ B-NF- κ B signaling module: temporal control and selective gene activation. *Science* 298, 1241–1245. <https://doi.org/10.1126/science.1071914>.
- Hyman, A.A., Weber, C.A., and Jülicher, F. (2014). Liquid-liquid phase separation in biology. *Annu. Rev. Cell Dev. Biol.* 30, 39–58. <https://doi.org/10.1146/annurev-cellbio-100913-013325>.
- Jensen, M.H., Sneppen, K., and Tiana, G. (2003). Sustained oscillations and time delays in gene expression of protein Hes1. *FEBS Lett.* 541, 176–177. [https://doi.org/10.1016/s0014-5793\(03\)00279-5](https://doi.org/10.1016/s0014-5793(03)00279-5).
- Kamagata, K., Kanbayashi, S., Honda, M., Itoh, Y., Takahashi, H., Kameda, T., Nagatsugi, F., and Takahashi, S. (2020). Liquid-like droplet formation by tumor suppressor p53 induced by multivalent electrostatic interactions between two disordered domains. *Sci. Rep.* 10, 580. <https://doi.org/10.1038/s41598-020-57521-w>.
- Kilic, S., Lezaja, A., Gatti, M., Bianco, E., Michelena, J., Imhof, R., and Altmeier, M. (2019). Phase separation of 53BP1 determines liquid-like behavior of DNA repair compartments. *EMBO J.* 38, e101379. <https://doi.org/10.1525/embj.2018101379>.
- Kim, J.K., Josić, K., and Bennett, M.R. (2015). The relationship between stochastic and deterministic quasi-steady state approximations. *BMC Syst. Biol.* 9, 87–13. <https://doi.org/10.1186/s12918-015-0218-3>.
- Kirschbaum, J., and Zwicker, D. (2021). Controlling biomolecular condensates via chemical reactions. *J. R. Soc. Interface* 18, 20210255. <https://doi.org/10.1098/rsif.2021.0255>.
- Kobayashi, T., Mizuno, H., Imayoshi, I., Furusawa, C., Shirahige, K., and Kageyama, R. (2009). The cyclic gene Hes1 contributes to diverse differentiation responses of embryonic stem cells. *Genes Dev.* 23, 1870–1875. <https://doi.org/10.1101/gad.1823109>.
- Lahav, G., Rosenfeld, N., Sigal, A., Geva-Zatorsky, N., Levine, A.J., Elowitz, M.B., and Alon, U. (2004). Dynamics of the p53-Mdm2 feedback loop in individual cells. *Nat. Genet.* 36, 147–150. <https://doi.org/10.1038/ng1293>.
- Larson, A.G., Elnatan, D., Keenen, M.M., Trnka, M.J., Johnston, J.B., Burlingame, A.L., Agard, D.A., Redding, S., and Narlikar, G.J. (2017). Liquid droplet formation by HP1 α suggests a role for phase separation in heterochromatin. *Nature* 547, 236–240. <https://doi.org/10.1038/nature22822>.
- Lifshitz, I., and Slyozov, V. (1961). The kinetics of precipitation from supersaturated solid solutions. *J. Phys. Chem. Solid.* 19, 35–50. [https://doi.org/10.1016/0022-3697\(61\)90054-3](https://doi.org/10.1016/0022-3697(61)90054-3).
- Lisby, M., Barlow, J.H., Burgess, R.C., and Rothstein, R. (2004). Choreography of the DNA damage response: spatiotemporal relationships among checkpoint and repair proteins. *Cell* 118, 699–713. <https://doi.org/10.1016/j.cell.2004.08.015>.
- Matsuda, T., Miyawaki, A., and Nagai, T. (2008). Direct measurement of protein dynamics inside cells using a rationally designed photoconvertible protein. *Nat. Methods* 5, 339–345. <https://doi.org/10.1038/nmeth.1193>.
- Mengel, B., Hunziker, A., Pedersen, L., Trusina, A., Jensen, M.H., and Krishna, S. (2010). Modeling oscillatory control in NF- κ B, p53 and Wnt signaling. *Curr. Opin. Genet. Dev.* 20, 656–664. <https://doi.org/10.1016/j.gde.2010.08.008>.
- Miné-Hattab, J., Heltberg, M., Villemeur, M., Guedj, C., Mora, T., Walczak, A.M., Dahan, M., and Taddei, A. (2021). Single molecule microscopy reveals key physical features of repair foci in living cells. *Elife* 10, e60577. <https://doi.org/10.7554/elife.60577>.
- Mohseni-Salehi, F.S., Zare-Mirakabad, F., Sadeghi, M., and Ghafouri-Fard, S. (2020). A Stochastic Model of DNA Double-Strand Breaks Repair Throughout the Cell Cycle. *Bull. Math. Biol.* 82, 11. <https://doi.org/10.1007/s11538-019-00692-z>.
- Nelson, D.E., Ihekwaba, A.E.C., Elliott, M., Johnson, J.R., Gibney, C.A., Foreman, B.E., Nelson, G., See, V., Horton, C.A., Spiller, D.G., et al. (2004). Oscillations in NF- κ B Signaling Control the Dynamics of Gene Expression. *Science* 306, 704–708. <https://doi.org/10.1126/science.1099962>.
- Nishanov, V.N., and Sobyanin, A.A. (1986). Diffusive decay of the metastable state in periodic field. *Phys. Status Solidi* 95, 41–50. <https://doi.org/10.1002/pssa.2210950103>.
- Oshidari, R., Huang, R., Medghalchi, M., Tse, E.Y.W., Ashgriz, N., Lee, H.O., Wyatt, H., and Mekhail, K. (2020). DNA repair by Rad52 liquid droplets. *Nat. Commun.* 11, 695. <https://doi.org/10.1038/s41467-020-14546-z>.
- Pessina, F., Giavazzi, F., Yin, Y., Gioia, U., Vitelli, V., Galbiati, A., Barozzi, S., Garre, M., Oldani, A., Flaus, A., et al. (2019). Functional transcription promoters at DNA double-strand breaks mediate RNA-driven phase separation of damage-response factors. *Nat. Cell Biol.* 21, 1286–1299. <https://doi.org/10.1038/s41556-019-0392-4>.
- Petronilho, E.C., Pedrote, M.M., Marques, M.A., Passos, Y.M., Mota, M.F., Jakobus, B., Sousa, G.d.S.d., Pereira da Costa, F., Felix, A.L., Ferretti, G.D.S., et al. (2021). Phase separation of p53 precedes aggregation and is affected by oncogenic mutations and ligands. *Chem. Sci.* 12, 7334–7349. <https://doi.org/10.1039/d1sc01739j>.
- Reyes, J., Chen, J.-Y., Stewart-Ornstein, J., Karhohs, K.W., Mock, C.S., and Lahav, G. (2018). Fluctuations in p53 signaling allow escape from cell-cycle arrest. *Mol. Cell* 71, 581–591.e5. <https://doi.org/10.1016/j.molcel.2018.06.031>.
- Schindelin, J., Arganda-Carreras, I., Frise, E., Kaynig, V., Longair, M., Pietzsch, T., Preibisch, S., Rueden, C., Saalfeld, S., Schmid, B., et al. (2012). Fiji: an open-source platform for biological-image analysis. *Nat. Methods* 9, 676–682. <https://doi.org/10.1038/nmeth.2019>.
- Schmidt, U., Weigert, M., Broaddus, C., and Myers, G. (2018). Cell detection with star-convex polygons. *International Conference on Medical Image Computing and Computer-Assisted Intervention (Springer)*, pp. 265–273. https://doi.org/10.1007/978-3-030-00934-2_30.
- Stewart-Ornstein, J., and Lahav, G. (2017). p53 dynamics in response to DNA damage vary across cell lines and are shaped by efficiency of DNA repair and activity of the kinase ATM. *Sci. Signal.* 10, eaah6671. <https://doi.org/10.1126/scisignal.aah6671>.

- Strom, A.R., Emelyanov, A.V., Mir, M., Fyodorov, D.V., Darzacq, X., and Karpen, G.H. (2017). Phase separation drives heterochromatin domain formation. *Nature* 547, 241–245. <https://doi.org/10.1038/nature22989>.
- Sun, H.B., Shen, J., and Yokota, H. (2000). Size-Dependent Positioning of Human Chromosomes in Interphase Nuclei. *Biophys. J.* 79, 184–190. [https://doi.org/10.1016/s0006-3495\(00\)76282-5](https://doi.org/10.1016/s0006-3495(00)76282-5).
- Söding, J., Zwicker, D., Sohrabi-Jahromi, S., Boehning, M., and Kirschbaum, J. (2020). Mechanisms for Active Regulation of Biomolecular Condensates. *Trends Cell Biol.* 30, 4–14. <https://doi.org/10.1016/j.tcb.2019.10.006>.
- Tiana, G., Jensen, M.H., and Sneppen, K. (2002). Time delay as a key to apoptosis induction in the p53 network. *Eur. Phys. J. B* 29, 135–140. <https://doi.org/10.1140/epjb/e2002-00271-1>.
- Wagner, C. (1961). Theorie der Alterung von Niederschlägen durch Umlösen (Ostwald-Reifung). *Ber. Bunsen Ges. Phys. Chem.* 65, 581–591. <https://doi.org/10.1002/bbpc.19610650704>.
- Wang, Y.-H., Ho, T.L.F., Hariharan, A., Goh, H.C., Wong, Y.L., Verkaik, N.S., Lee, M.Y., Tam, W.L., van Gent, D.C., Venkitaraman, A.R., et al. (2022a). Rapid recruitment of p53 to DNA damage sites directs DNA repair choice and integrity. *Proc. Natl. Acad. Sci. USA* 119, e2113233119. <https://doi.org/10.1073/pnas.2113233119>.
- Wang, Y.L., Zhao, W.W., Bai, S.M., Feng, L.L., Bie, S.Y., Gong, L., Wang, F., Wei, M.B., Feng, W.X., Pang, X.L., et al. (2022b). MRNIP condensates promote DNA double-strand break sensing and end resection. *Nat. Commun.* 13, 2638. <https://doi.org/10.1038/s41467-022-30303-w>.
- Weber, C.A., Zwicker, D., Jülicher, F., and Lee, C.F. (2019). Physics of active emulsions. *Rep. Prog. Phys.* 82, 064601. <https://doi.org/10.1088/1361-6633/ab052b>.
- Webster, A.J., and Cates, M.E. (2001). Osmotic stabilization of concentrated emulsions and foams. *Langmuir* 17, 595–608. <https://doi.org/10.1021/la000699m>.
- Xin, H.L., and Zheng, H. (2012). In situ observation of oscillatory growth of bismuth nanoparticles. *Nano Lett.* 12, 1470–1474. <https://doi.org/10.1021/nl2041854>.
- Yang, R., Huang, B., Zhu, Y., Li, Y., Liu, F., and Shi, J. (2018). Cell type-dependent bimodal p53 activation engenders a dynamic mechanism of chemoresistance. *Sci. Adv.* 4, eaat5077. <https://doi.org/10.1126/sciadv.aat5077>.
- Zwicker, D., Hyman, A.A., and Jülicher, F. (2015). Suppression of Ostwald ripening in active emulsions. *Phys. Rev. E Stat. Nonlin. Soft Matter Phys.* 92, 012317. <https://doi.org/10.1103/PhysRevE.92.012317>.

STAR★METHODS

KEY RESOURCES TABLE

REAGENT or RESOURCE	SOURCE	IDENTIFIER
Antibodies		
Anti-phospho-Histone H2A.X (Ser139) Antibody, clone JBW301	Millipore	Cat#05–636; RRID: AB_309864
Goat anti-Mouse IgG (H + L) Highly Cross-Adsorbed Secondary Antibody, Alexa Fluor Plus 647	Invitrogen	Cat#A32728; RRID: AB_2633277
Chemicals, peptides, and recombinant proteins		
Neocarzinostatin from Streptomyces carzinostaticus	Sigma-Aldrich	Cat#N9162
Nutlin-3a	Sigma-Aldrich	Cat#SML0580
DAPI [4,6-Diamidino-2-phenylindole, dihydrochloride]	AAT Bioquest	Cat#17510
Paraformaldehyde 16% (w/v) in aqueous solution methanol-free	Thermo Scientific Chemicals	Cat#43368
DPBS (10X), no calcium, no magnesium	Gibco	Cat#14200075
RPMI 1640 Media	Gibco	Cat#11875093
Antibiotic-Antimycotic (100X)	Gibco	Cat#15240062
Characterized FBS, Canadian Origin	HyClone	Cat#SH30396.03
Albumin, Bovine Serum, Fraction V, low Heavy Metals (BSA)	MerckMillipore	Cat#12659
Triton X-100 Reagent Grade	BioShop	Cat#TRX506
SiR700-DNA Kit	Spirochrome	Cat#SC015
Experimental models: Cell lines		
A172	ATCC	Cat#CRL-1620; RRID: CVCL_0131
A549	ATCC	Cat#CCL-185; RRID: CVCL_0023
HCT116	ATCC	Cat#CCL-247; RRID: CVCL_0291
hTERT RPE-1	ATCC	Cat#CRL-4000; RRID: CVCL_4388
U2OS	ATCC	Cat#HTB-96; RRID: CVCL_0042
MCF7+p53shRNA + p53-mCerulean	Gaglia et al. (2013)	N/A
A549+UbCp-p53-mVenus	Stewart-Ornstein and Lahav (2017)	N/A
RPE-1+UbCp-p53-mNeonGreen	Reyes et al. (2018)	N/A
Software and algorithms		
MATLAB (2020b)	The Mathworks	https://MATLAB.mathworks.com/
Single cell tracking algorithm	Reyes et al. (2018)	https://github.com/balvalhal/p53CinemaManual
Fiji	Schindelin et al. (2012)	https://fiji.sc/
StarDist	Schmidt et al. (2018)	https://github.com/stardist/stardist
γH2AX foci quantification algorithm	This paper	N/A

RESOURCE AVAILABILITY

Lead contact

Further information and requests for resources should be directed to and will be fulfilled by the lead contact, Mogens H. Jensen (mhjensen@nbi.dk).

Materials availability

All materials are commercially available.

Data and code availability

- All data reported in this paper will be shared by the [lead contact](#) upon request.
- All software and code used in this study are available through a Github repository at <https://github.com/MathiasHeltberg/EnhancedDNARepairThroughDropletFormationAndp53Oscillations>.
- Any additional information required to reproduce the simulations and reanalyze the data reported in this paper are available from the [lead contact](#) upon request.

EXPERIMENTAL MODEL AND SUBJECT DETAILS

Cell culture

All cell lines were adopted and maintained in RPMI 1640 media supplemented with 5% FBS and antibiotics (Streptomycin, Amphotericin B, Penicillin). Cells were grown in the humidified incubator at 37°C with 5% CO₂.

METHOD DETAILS

Live cell imaging

A549 and RPE-1 p53 reporter cells were seeded at 2x103 cells/well in a μ-Plate 96 Well Black plate (ibidi Cat#89626) 1 day before imaging with Nikon Eclipse Ti inverted microscope. Cells were switched to transparent RPMI (RPMI without riboflavin and phenol red, customized by US Biological) 1 h before imaging and SiR700 DNA probe (1:40,000) was added to label nuclei for single-cell tracking purposes. During imaging, cells were maintained in a chamber controlling CO₂ (5%), temperature (37°C), and humidity. Images were acquired every 30 min with appropriate filter sets: SiR700 (ex:640/30; em:700/75) and p53 (ex:510/25; em:544/24). NCS was added to induce oscillatory p53 dynamics. To achieve sustained p53 levels, 0.75 and 0.55 μM Nutlin-3a were added 2.5 and 5.5h after NCS treatment, respectively.

Single cell tracking and p53 level quantification

Individual cells were tracked using a semi-automated MATLAB program described previously ([Reyes et al., 2018](#)). p53 level was quantified by averaging the p53 signals within the cell nucleus. Individual p53 traces were smoothed using a 1h sliding window.

Immunofluorescence

Cells were seeded at 2x103 cells/well in 96-Well Micro-Well Plates (Nunc Catt#167008) 2 days before NCS treatment. After treatment, cells were fixed at indicated time in 4% paraformaldehyde for 10 min, washed three times with PBS, and then permeabilized with PBS containing 1% Triton X-100 for 5 min at room temperature. After permeabilization, cells were blocked in antibody dilution buffer (2% BSA and 0.1% Triton X-100 in PBS) for 1 h, followed by primary antibody (Anti-phospho-Histone H2A.X Ser139, 1:1000) incubation overnight at 4°C. Cells were then washed three times in PBS, incubated in antibody dilution buffer containing secondary antibodies (Goat anti-Mouse Alexa FluorPlus 647, 1:1000) for 1 h, followed by DAPI staining (5 μg/ml in PBS) for 5 min at room temperature. Cells were washed three times with PBS and imaged with ImageXpress Micro XL High-Content Screening System (Molecular Device). The filter settings: Cy5 (ex:628/40; em:692/40) and DAPI (ex:377/50; em:447/60).

γ-H2AX foci quantification

Cell nuclei were segmented according to DAPI signals using StarDist ([Schmidt et al., 2018](#)), a plugin for Fiji ([Schindelin et al., 2012](#)). Images of the γ-H2AX (Cy5 channel) were background subtracted (rolling ball radius: 50 pixels) prior to quantification. γ-H2AX foci were quantified using custom MATLAB scripts. Generally, within each nucleus, Cy5 intensities below an absolute intensity threshold were filtered out. For nuclei with strong Cy5 background, the intensities were normalized to range between 0 and 1 and pixels below a normalized intensity threshold were filtered out. Peaks of Cy5 intensities with prominences above a threshold were detected using the findpeaks function in MATLAB. The coefficient of variation (CV) in intensity between each detected peak and its adjacent pixels were taken. Peaks with CV above a threshold stood out well from its surrounding and therefore were considered as γ-H2AX foci centroids. The number of such centroids in each nucleus represented the number of presenting γ-H2AX foci. All thresholds were determined manually for each cell line to best match visual inspection of γ-H2AX foci.

Parameter estimates

- D: The diffusion coefficient in the nucleus. This has been thoroughly investigated in the past, and even though it differs for different types of proteins, it can be roughly approximated as $D \approx 10 \mu\text{m}^2\text{s}^{-1}$.
- D_0 : The diffusion coefficient inside the focus. This has been estimated in the work of [Miné-Hattab et al. \(2021\)](#), where it is shown to be 1/100 D. Even though it might vary for different types of proteins, this should reflect the right order of magnitude.
- c_{in} : The protein concentration inside droplets. [Söding et al. \(2020\)](#) estimate the internal concentration of biomolecular condensates, assuming a 1:1 protein to water ratio, a protein density similar to water and a protein molecular weight of 30kDa, obtaining $c_{in} \approx 17 \text{ mM}$. This corresponds to $\approx 10^7 \text{ molecules } \mu\text{m}^{-3}$. In order to confine the search, we have fixed $c_{in} \approx 10^6 \mu\text{m}^{-3}$.

- l_γ : The capillary length of the droplets. This is typically estimated to follow the relation: $l_\gamma \approx (2\gamma / c_{in} k_B T)$, with γ being the surface tension of the droplets. From the work of [Pessina et al. \(2019\)](#) γ is roughly $0.1 \mu Nm^{-1}$, which together with the previous estimate of c_{in} , define a physiological value for l_γ .
- c_{out} : The protein concentration outside droplets. We know that in a supersaturated environment proteins are enriched in the condensates. [Söding et al. \(2020\)](#) estimate the ratio of $c_{in}/c_{out} \approx 100$. In our paper, again to confine the search, we fixed this ratio to 1000.
- N : The number of foci arising as a result of DNA damage has been measured by [Pessina et al. \(2019\)](#) to be approximately 30, and anyway in the range 10–100, therefore we also considered values in this range.
- ω : The p53 periodicity has extensively been measured in the past ([Lahav et al., 2004](#)).
- \bar{c} : We have fixed the average concentration of repair proteins to be close to c , so that the oscillations of p53 of the right amplitude would make the environment oscillate between being supersaturated and undersaturated.
- A : We have varied the amplitude of the oscillations in a range such that the ratio \bar{c}_0/A_c would be consistent with the ratio of p53 mean level and amplitude.
- M : The number of steps necessary to repair the DNA damages. [Hahnfeldt et al. \(1992\)](#) modeled the evolution of DNA damage in irradiated cells as a Markov chain, in which several steps had to be accomplished to achieve full repair. In a recent biophysical work ([Mohseni-Salehi et al., 2020](#)), the DNA repair process is modeled as a Markov chain and the number of possible steps is estimated to be around 20.
- λ : The rate of damage recreation. We assumed that, along with the correct repair mechanisms, “misrepair events” may also occur, such as mistakes by the repair enzymes or a gradual loss of a lesion’s ability to undergo any reaction ([Hahnfeldt et al., 1992](#)). This parameter is not strictly relevant for the conclusions of our work, therefore is assumed to be small for the majority of the simulations. It only serves the purpose to define a timescale for repair processes to be completed.

First passage time in the Smoluchowski limit

In the following we describe the rate of capture for a diffusing molecule, that can get absorbed by (i.e. react with) another molecule. We write up the Smoluchowski equation in spatial coordinates assuming angular symmetry. In the stationary state this takes the form

$$0 = \nabla \cdot D(r)(\nabla - \beta F(r))p(r),$$

with the two boundary conditions:

$$p(r \mapsto \infty) = c_1 c_2$$

$$D(R_0)(\nabla - \beta F(R_0))p(R_0, t) = \kappa p(R_0)$$

The first guarantees a constant concentration of molecules away from the sphere of interest and the second is the radiation Boundary Condition. The parameter κ defines the absorbance of the binding site. Integrating with respect to the volume and applying Gauss theorem yields

$$\int_V \nabla \cdot D(r)(\nabla - \beta F(r))p(r, t) dV = 4\pi r^2 D(r)(\nabla - \beta F(r))p(r, t)$$

Next, inserting the Boundary Condition 2) and rewriting the first term gives

$$\partial_r (e^{\beta U(r)} p(r)) = \frac{R_0^2 \kappa}{r^2 D(r)} e^{\beta U(r)} p(R_0).$$

Integrating on both sides, from R_0 to ∞ results in

$$\frac{c_1 c_2}{\left(e^{-\beta U(R_0)} R_0^2 \kappa \int_{R_0}^{\infty} \frac{1}{r^2 D(r)} e^{\beta U(r)} dr + 1 \right)} e^{-\beta U(R_0)} = p(R_0).$$

The total radial current into the partially absorbing sphere is equivalent to the rate of absorption:

$$I_{rad} = k^* = 4\pi R_0^2 \kappa p(R_0) = 4\pi R_0^2 \kappa \frac{c_1 c_2}{\left(e^{-\beta U(R_0)} R_0^2 \kappa \int_{R_0}^{\infty} \frac{1}{r^2 D(r)} e^{\beta U(r)} dr + 1 \right)} e^{-\beta U(R_0)}.$$

We define the actual on-rate as a constant multiplied by the concentrations of the two interacting molecules: $k^* = k^+ c_1 c_2$. Therefore removing the dependencies on c_1 and c_2 yields

$$k^+ = \frac{4\pi}{\left(\int_{R_0}^{\infty} \frac{1}{r^2 D(r)} e^{\beta U(r)} dr + \frac{e^{\beta U(R_0)}}{R_0^2 \kappa} \right)}.$$

If we assume that $\kappa \approx 0$ we note that we recover the Arrhenius equation. Assuming diffusion limited reactions (i.e. $U(r) \approx 0$) we get:

$$k^+ = \frac{4\pi}{\int_{R_0}^{\infty} \frac{1}{r^2 D_0} dr + \frac{1}{R_0^2 \kappa}} = \frac{4\pi D_0 R_0}{1 + \frac{D_0}{R_0 \kappa}}.$$

We see that we here arrive at the diffusion limited reaction rate ($k^+ = 4\pi D_0 R_0$) if we also assume that $\kappa \rightarrow \infty$. We note here that the classical result derived by Berg and Purcell, where one assumes a surface of small absorbing disks, leads to an on-rate of

$$k_{BP}^+ = 4\pi D R_0 \frac{Na}{\pi R_0 + Na}$$

where a is the radius of the small disks covering the absorbing spheres. These two expressions are therefore equivalent if $\kappa = (NaD / \pi R_0^2)$. We now assume that the absorbing center is in the middle of a liquid droplet, which we model by a spherically symmetric potential $U(r)$. The probability distribution of a molecule is denoted by $p(r) = p(r)$. The probability density of being at distance r from the absorbing site is given by $q(r) = 4\pi r^2 p(r)$. At steady state with a non-vanishing flux $J = \text{const}$, we have:

$$\left(\frac{2D}{r} - \frac{D}{k_B T} \partial_r U \right) q = D \partial_r q - J.$$

Introducing the variable $\varphi = -2\ln(r) + U/kBT$, we simplify this as:

$$q \partial_r \varphi + \partial_r q = \frac{J}{D}.$$

By multiplication with e^φ , we obtain:

$$\partial_r (e^\varphi q) = \frac{J}{D} e^\varphi.$$

The general solution to that equation is:

$$q(r) = C e^{-\varphi(r)} + J e^{-\varphi(r)} \int_{r_0}^r \frac{e^{\varphi(r')}}{D(r')} dr'.$$

Here $C = 0$ due to the absorbing boundary condition $q(r_0) = 0$. The constant J is determined by the normalization $\int_{r_0}^r dr q(r) = 1$ yielding:

$$J^{-1} = \tau_a = \int_{r_0}^{r_n} dr e^{-\varphi(r)} \int_{r_0}^{r_n} dr' \frac{e^{\varphi(r')}}{D(r')},$$

By replacing $\varphi(r)$ by its definition and assuming a strong surface potential of the liquid droplet we directly retrieve [Equation 3](#).

Derivation of droplet growth

We first describe an infinite system with two inhomogeneous phases, whose free energy F is therefore given by

$$F = V_1 f(c_1) + V_2 f(c_2),$$

where f is the free energy density, $V_{1,2}$ are the volumes of the two phases and $c_{1,2}$ are the respective equilibrium concentrations. Assuming that the total volume is constant and that the number of molecules is fixed leads to $V_T = V_1 + V_2$ and $c_T V_T = V_1 c_1 + V_2 c_2$, with V_T being the total volume and c_T the average concentration. Thus F can be written in terms of c_1, V_1, c_T, V_T as

$$F = V_1 f(c_1) + (V_T - V_1) f\left(\frac{c_T V_T - V_1 c_1}{V_T - V_1}\right).$$

The stability of the inhomogeneous state corresponds to a minimum of the free energy in terms of the concentration and the volume of the first phase. Therefore we differentiate the free energy with respect to c_1 and V_1 and equate these to zero, which yields

$$\partial_{c_1} F = 0 \Rightarrow f'(c_1) - f'(c_2) \cdot [c_2 - c_1] = 0, \quad (\text{S1})$$

$$\partial_{V_1} F = 0 \Rightarrow f(c_1) - f(c_2) + f'(c_2) \cdot [c_2 - c_1] = 0. \quad (\text{S2})$$

Being in the thermodynamic limit, we have been entitled up to now to ignore surface effects. On the contrary, these play a major role in the regime of droplets, where the free energy portrays an additional term ($+A\gamma$, with A being the area of the interface and γ the surface tension). Therefore, in the case of a spherical droplet, the free energy takes the form:

$$F = V_d f(c_{in}) + (V - V_d) f(c_{out}) + 4\pi R^2 \gamma,$$

where $V_d = (4\pi/3)R^3$ is the volume of a spherical droplet of radius R , $c_{in/out}$ are the internal/external concentrations and V is the total volume of the system. With similar reasoning as before, we differentiate with respect to c_{in} and V_d , which results in

$$0 = f'(c_{in}^{eq}) - f'(c_{out}^{eq}),$$

$$0 = f(c_{in}^{eq}) - f(c_{out}^{eq}) + (c_{out}^{eq} - c_{in}^{eq}) f'(c_{out}^{eq}) + \frac{2\gamma}{R},$$

where $c_{in/out}^{eq}$ are the internal/external equilibrium concentrations. We see that the last term (known as the Laplace pressure) is negligible in the thermodynamic limit, in which case we retrieve [Equations S1](#) and [S2](#). At this point we could write the equilibrium concentrations as a first order correction of the correspondent concentration in the thermodynamic limit ($c_{in/out}^{(0)}$), such that $c_{in/out}^{eq} = c_{in/out}^{(0)} + \delta c_{in/out}$. In this way we derive the following expressions:

$$c_{out}^{eq} = c_{out}^{(0)} \cdot \left(1 + \frac{l_\gamma}{R}\right), \quad (\text{S3})$$

$$c_{in}^{eq} \approx c_{in}^{(0)}, \quad (\text{S4})$$

with l_γ defined as the capillary length and the latter expression holding since we consider the case $c_{in}^{(0)} \gg c_{out}^{(0)}$.

We now seek to find an expression for the concentration c of molecules at some distance r from a single droplet of radius R embedded in an infinite medium, knowing that the concentration far away from the droplet is fixed to c_∞ . Given the symmetry of the system, c will only be a function of r . We further assume that the droplet radius varies slowly such that it can be considered constant on the timescale of the diffusing molecules. The concentration gradient then causes a net diffusive flux density through a spherical shell of radius r given by $j(r) = -D \frac{\partial}{\partial r} c(r)$ with D being the diffusion coefficient. Given that the number of molecules is fixed, the total flux across shell surfaces of radius r must be constant, and given by

$$J = -4\pi D r^2 \frac{\partial}{\partial r} c(r) = \text{const.}$$

This equation has solution $c(r) = k_1 + k_2/r$, with constants $k_{1,2}$ given by the boundary conditions at R and ∞ ($c(R) = c_{out}^{eq}$ as defined in [Equation S3](#) and $c(\infty) = c_\infty$). Therefore the solution reads

$$\begin{aligned} c(r) &= c_\infty + (c_{out}^{eq} - c_\infty) \frac{R}{r} & r > R, \\ c(r) &= c_{in}^{eq} r < R. \end{aligned}$$

The total flux of molecules leaving the droplet is

$$J_R = 4\pi D R^2 \frac{\partial}{\partial r} c(r) |_{r=R} = -4\pi D R (c_{out}^{eq} - c_\infty). \quad (\text{S5})$$

The variation of the droplet volume is given by $(dV_d/dt) = J_R/c_{in}^{eq}$, that is

$$\frac{d}{dt} \left(\frac{4\pi}{3} R^3 \right) = -\frac{1}{c_{in}^{eq}} 4\pi D R (c_{out}^{eq} - c_\infty),$$

which, rearranged in terms of dR/dt and written in terms of $c_{in/out}^{(0)}$ yields

$$\frac{dR}{dt} = \frac{D c_{out}^{(0)}}{R c_{in}^{(0)}} \left(\frac{c_\infty}{c_{out}^{(0)}} - 1 - \frac{l_\gamma}{R} \right)$$

This expression can be easily generalized in case of N droplets far apart from each other, so that direct interactions can be neglected, while droplets only compete for material exchanging it through the common media. This directly yields [Equation 1](#) and [Equation 2](#) in the main text, where, for simplicity of notation, we have defined $c_{in/out}^{(0)}$ as $c_{in/out}$.

Simulation of droplet growth and damage repair with the Gillespie algorithm

Let us first consider an initial distribution of proteins $n_i \forall i = 1, \dots, N$, and then, given the assumptions of a constant internal concentration c_{in} (such that $V_i = n_i/c_{in}$), and spherical droplets, each radius R_i is computed accordingly as

$$R_i = \left(\frac{3n_i}{4\pi c_{in}} \right)^{1/3}.$$

The concentration far away from each droplet c_∞ is adjusted in order to ensure the mass conservation as

$$c_\infty = \frac{\bar{c}V_n - \sum_i n_i}{V_n - \frac{1}{c_{in}} \sum_i n_i}.$$

The flux of proteins in and out of the droplets is given by [Equation S5](#), while at the same time damage can be repaired or re-created. This gives rise to four possible processes for the i -th droplet, whose rates are

1. Growth of droplet by addition of one protein: $r_{1,i} = 4\pi D(c_\infty - c_{out})R_i$
2. Shrinkage of droplet by removal of one protein: $r_{2,i} = 4\pi Dc_{out}l_\gamma$
3. One step of damage repair: $r_{3,i} = 1/\tau$
4. One step of damage recreation: $r_{4,i} = \lambda$

Therefore we can include the rates (here denoted $\mu_i \in [r_{1,i}, r_{2,i}, r_{3,i}, r_{4,i}]$) of all the possible events and calculate the time until the next event as

$$T_{event} = \frac{-\ln(\mathcal{R})}{\sum \mu_i}, \quad (S6)$$

where \mathcal{R} is a random number, uniformly distributed between 0 and 1. Then, in order to find which of the possible events take place, we assign a number to each reaction rate and choose the reaction, m , that satisfies:

$$\frac{\sum_{i=1}^{m-1} \mu_i}{\sum_{i=1}^N \mu_i} \leq \mathcal{R} \leq \frac{\sum_{i=1}^m \mu_i}{\sum_{i=1}^N \mu_i} \quad (S7)$$

After each event we update all the rates, and then repeat the steps. With this algorithm one can therefore simulate the system, based on single proteins dynamics, in the presence of intrinsic noise. We note that since our equations have been derived in the quasi-steady state approximation, the direct application of the Gillespie algorithm can lead to inaccurate estimation of the noise level, in general to an underestimation of stochasticity compared to the full system ([Kim et al., 2015](#)). However, this potential imprecision does not affect the main results, since the stochasticity is mainly responsible for generating a mixed initial state and the very early growth of the droplets. As soon as the droplets get past this initial phase, the forces are so strong that the stochasticity only plays a minor role. Having higher noise would result in an earlier dominance of Ostwald ripening, since the fluctuations could in principle drive the system out of the metastable state in which some droplets temporarily co-exist. This would further enhance the need for an oscillatory mechanism to prevent the effect of Ostwald ripening.

Transition from diffusion to Ostwald ripening

Material flux from far away toward the droplets surface ceases when the gradient of concentration is null, that is when $c_\infty \approx c_{out}$. Considering the same initial radius $R_i \approx 0 \forall i$ one can assume that all droplets roughly reach the same size at that point, so that

$\sum_{i=1}^N V_i = N \cdot V_i$. In this case [Equation 2](#) takes the form

$$\bar{c}V = c_{in}N \cdot V_i + c_{out}V - c_{out}N \cdot V_i.$$

Isolating for V_i and considering that $c_{in} \gg c_{out}$ directly yields [Equation 6](#).

Ostwald Ripening timescale of coarsening

By considering the definition of the critical radius

$$R_c = \frac{c_{out}}{c_\infty - c_{out}} l_\gamma,$$

it is possible to express [Equation 1](#) as

$$(dR / dt) = (Dl_r / R^2 R_c)(c_{out} / c_{in})(R - R_c).$$

Moreover, considering that R_c changes much more slowly than R

$$\frac{dR}{dt} \approx \frac{d(R - R_c)}{dt} = \frac{1}{T_{OR}}(R - R_c),$$

with T_{OR} being the timescale of coarsening as defined in [Equation 7](#).

Visualizing p53 dynamics in polar coordinates

The p53 and Mdm2 levels are first centered around their mean values such that $x = p53 - \langle p53 \rangle$ and $y = Mdm2 - \langle Mdm2 \rangle$, which are then transformed in polar coordinates (r, θ) as $r = \sqrt{x^2 + y^2}$ and $\theta = \arctan(y/x)$. The angular space is then divided in 50 sections, within each of whom the mean and SD of the trajectories are calculated.

On non-linear p53 stimulation and the dependency of waveforms

In the paper we have investigated how the oscillations in p53 concentration affected the repair foci, generally assuming, for simplicity, a sinusoidal p53 signal and a linear relation with the droplet material concentration. In the following, we would first like to compare different types of waveforms on the resulting repair of damage. Secondly, we investigate the effect of non-linear relations between p53 and downstream droplet proteins, which would be a fair assumption if the main role of p53 were in the transcriptional-dependent processes.

To test the dependency of other waveforms on the Ostwald ripening, we considered three very distinct waveforms: sinusoidal, square and triangular waves. Keeping the frequency and amplitude fixed, we measured the repair efficiency for each of the waveforms ([Figure S1A](#)). Here we find that they all have a frequency dependency that enhances the repair efficiency and that this is very similar for the triangular and sinusoidal waveform, but covers a larger range of frequencies for the square wave. This is explained by the fact that the square wave will spend longer time at the maximal concentration level, that allows more droplets to co-exist and thereby enhancing the overall efficiency of repair.

Secondly, from a mathematical point of view, the dynamics of downstream proteins (denoted by L) leading to the liquid-liquid phase separation, would be given by

$$\dot{L} = f(p) - \delta L,$$

where we have assumed that L is spontaneously degraded at a rate δ , and that it is produced as a function of p53 (denoted by p). In the regime of biochemical functions, where we assume that p53 is not a repressor but an activator, we would demand that: 1) p is positive (since it is a concentration) 2) $f(p)$ is monotonically increasing (since it is an activator by definition). These two constraints allow us to distinguish four different cases for $f(p)$:

$$f''(p) = 0 \Rightarrow f(p) = cp$$

$$f''(p) > 0 \Rightarrow f(p) = cp^2$$

$$f''(p) < 0 \Rightarrow f(p) = \frac{p}{c+p}$$

$$f''(p) \begin{cases} > 0 \text{ for } p < c \\ < 0 \text{ for } p > c \end{cases} \Rightarrow f(p) = \frac{p^h}{c^h + p^h}$$

Here c is a positive parameter and h is the integer of a Hill function. For oscillatory levels of p53, we simulated the concentration of the protein L, which turned out to be itself oscillatory in each case, even though the shape of the waveforms may vary ([Figure S1B](#)). The only case where oscillations are completely absent is when $f(p) = \frac{p}{\epsilon+p}$, where $\epsilon \ll 1$. However, this is a very special case, and we would argue that it is more likely that downstream targets generally possess an oscillatory output. This means that for the majority of cases, oscillations in p53 would also lead to oscillations in the downstream targets.

QUANTIFICATION AND STATISTICAL ANALYSIS

To compare the experimentally found distributions we applied the Mann–Whitney–Wilcoxon two-sided test in [Figures 5B–5E](#). To compare the similarities of the distributions we applied the two sided KS test ([Figure 5F](#)). To compare the fully repaired cells, we used the Student's t test to compare the two numbers, assuming Poisson counting statistics in the single bin ([Figure 5G](#)).

Supplemental figures

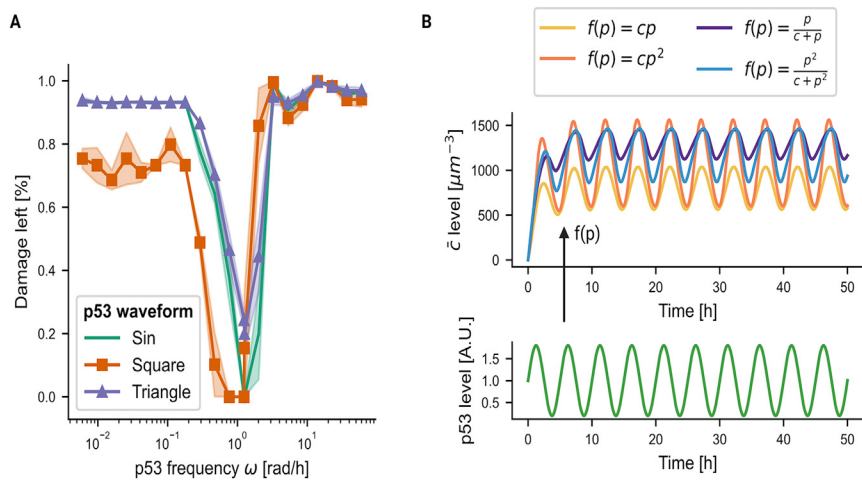


Figure S1. Effect of different p53 waveforms and non-linear relationship between p53 and droplet proteins concentration, related to STAR Methods

(A) Amount of damage left as a function of p53 frequency for three different p53 waveforms (sinusoidal, squared, triangular). (B) Oscillatory dynamics of p53 (below) and resulting average concentration of proteins, following 4 different types of stimulation.

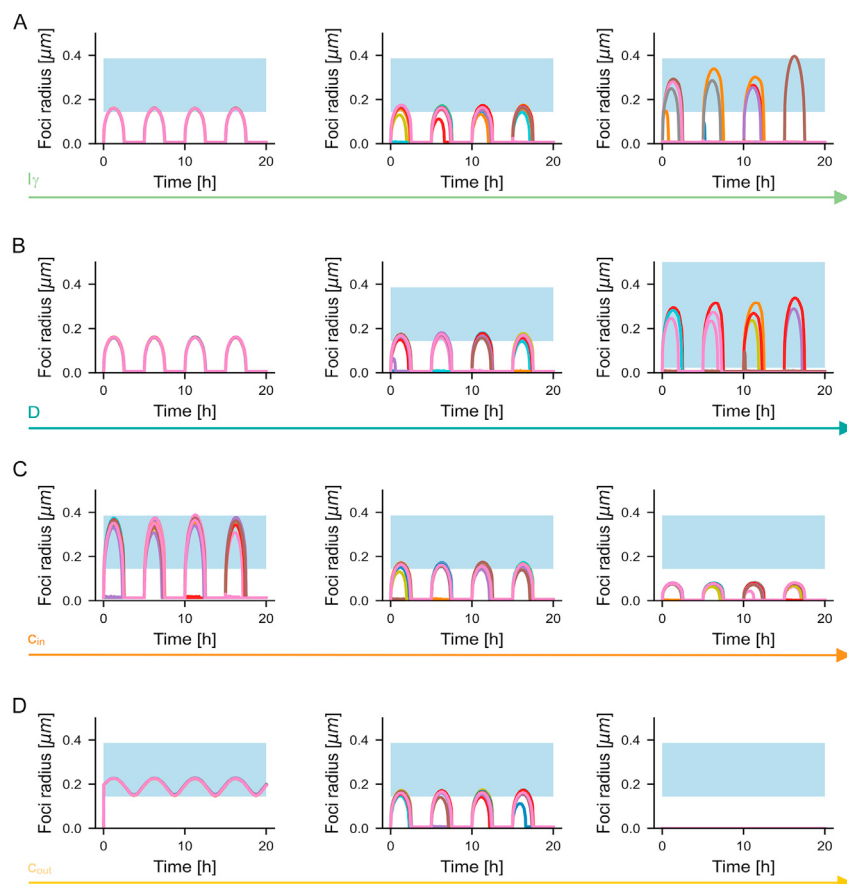


Figure S2. Effect of varying the parameters l_γ , D, c_{in} , and c_{out} on the timescale of coarsening, related to Figure 3

(A) Foci radius traces for increasing values of l_γ . The main effect is a shortening of the timescale of coarsening. (B) Same as (A), but for increasing values of D. The main effects are that the timescale of coarsening gets shorter and the optimal range gets wider. (C) Same as (A), but for increasing values of c_{in} . The main effect is that the resulting droplets are smaller, since the internal concentration is higher with the same average material. (D) Same as (A), but for increasing values of c_{out} . For $c_{out} < \bar{c}$ (left) the droplets are stabilized for long timescales, whereas for $c_{out} > \bar{c}$ (right) droplets cannot grow as the environment is undersaturated.

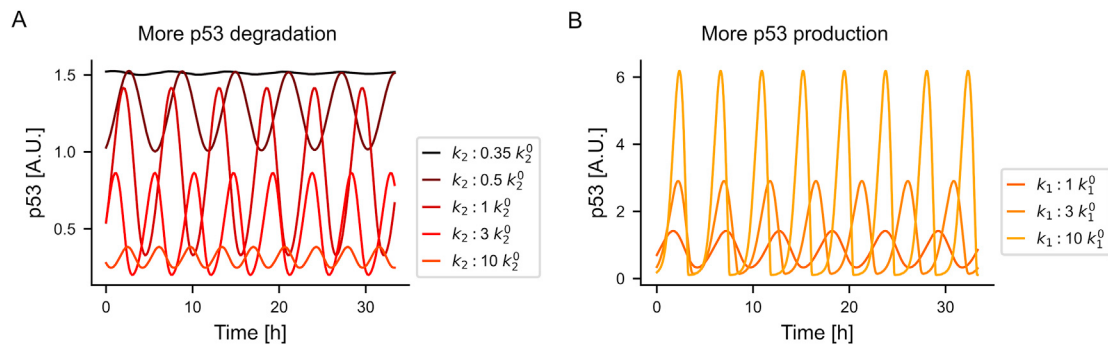


Figure S3. Different time series for p53 levels obtained by variation of the parameters k_2 and k_1 , related to Figure 4

(A) p53 level traces for increasing values of the degradation rate k_2 (with respect to a reference value k_2^0); low k_2 results in constant high levels for p53, while for higher k_2 a limit cycle with high amplitude oscillations emerges. (B) p53 level traces for increasing values of the production rate k_1 (with respect to a reference value k_1^0) show an increase in the amplitude of the oscillations.